Dynamics and thermodynamics of a pair of interacting magnetic dipoles

Heinz-Jürgen Schmidt[1] **, Christian Schröder**[2]**, Eva Hägele**[2] **and Marshall Luban**[3]

[1]Department of Physics, University of Osnabrück, D - 49069 Osnabrück, Germany
[2]Department of Engineering Sciences and Mathematics, University of Applied Sciences, D - 33692 Bielefeld, Germany
[3]Department of Physics and Astronomy, Iowa State University, Ames, IA 50011, USA

E-mail: hschmidt@uos.de

28 February 2015

Abstract. We consider the dynamics and thermodynamics of a pair of magnetic dipoles interacting via their magnetic fields. We consider only the "spin" degrees of freedom; the dipoles are fixed in space. With this restriction it is possible to provide the general solution of the equations of motion in analytical form. Thermodynamic quantities, such as the specific heat and the zero field susceptibility are calculated analytically or by combining low temperature asymptotic series and a complete high temperature expansion. The thermal expectation value of the autocorrelation function is determined for the low temperature regime and short times including terms linear in T. Furthermore, we have performed Monte Carlo simulations for the system under consideration and compared our analytical results with these.

PACS numbers: 75.75.Jn, 02.30lk, 75.40.Mg, 75.10.Hk

Keywords: Magnetic dipole-dipole interaction, integrable systems, Monte-Carlo simulation, high temperature expansion

Submitted to: *J. Phys. A: Math. Gen.*

1. Introduction

Systems in which magnetic nanostructures solely interact via electromagnetic forces have recently drawn much attention experimentally as well as theoretically [1] – [10]. Whereas in traditional magnetic systems electromagnetic forces usually just add to a complex exchange interaction scenario, they play a major role in arrays of interacting magnetic nanoparticles and lithographically produced nanostructures. In such systems geometrical frustration and disorder lead to interesting and exotic low temperature effects, e. g. artificial spin ice [11, 12], and superspin glass behavior [13]. Moreover, these systems are promising candidates for future applications beyond magnetic data-storage, e. g. , as low-power logical devices [14, 15]. Theoretically, these systems can often be described as interacting point dipoles. This is justified if the considered nanostructures form single domain magnets and are spatially well separated from each other so that exchange interactions do not play an important role. In this paper, we show that the dynamical and thermodynamical properties of the basic building block of such systems, a pair of interacting point dipoles, can rigorously be treated analytically by combining low temperature asymptotic series and a complete high temperature expansion. A considerable part of these calculations has been performed with the aid of the computer algebra system MATHEMATICA 9.0.

From a mathematical point of view, the system of two interacting magnetic dipoles is equivalent to a classical spin system with $N = 2$ and the particular XXZ Hamiltonian (12). Hence our results can be applied to these systems as well.

The paper is organized as follows. For the reader's convenience we recapitulate in section 2.1 the derivation of the equation of motion (eom) of two interacting dipoles and identify the underlying assumptions. The solution of the eom in terms of elliptic integrals and the Weierstrass elliptic function in sections 2.2 and 2.3 is based on the existence of two conserved quantities. The limiting case of solutions close to the ground state can be described by harmonic oscillations with three frequencies, see section 2.4. In the next sections we discuss the thermodynamics of the dipole pair. After explaining our methods we calculate the density of states function (section 3.2), the partition function (section 3.3), the specific heat (section 3.4) and the zero field susceptibility (section 3.5) by combining analytical methods with low- and high-temperature expansions. The latter two physical properties are also determined by Monte Carlo simulations and shown to closely coincide with the theoretical results. Since the problem is anisotropic we have to distinguish between different susceptibilities w. r. t. the "easy axis", the axis joining the two dipoles, and the "hard axis", any axis perpendicular to the easy axis. For the easy axis susceptibility there occur complications for the standard Monte Carlo simulations that have been overcome by using the so-called Exchange Monte Carlo method, see [17]. Similarly the autocorrelation function is calculated in the low temperature limit and compared with simulation results at low temperatures, see section 3.6. We find that one

of the three frequencies mentioned above is suppressed by thermodynamical averaging. For long times the autocorrelation function relaxes to constant values, see section 3.6.2. Appendix A contains a short introduction into the theory of elliptic integrals and elliptic functions for those readers who are not acquainted with this subject. The Appendices B – D contain details of the theoretical derivations presented in the main part of the paper. We close with a summary and outlook.

2. Dynamics

2.1. Derivation of the equation of motion

We consider two identical magnetic dipoles, labeled by an index $i = 1, 2$, that are fixed in space and separated by a distance a. We denote the magnetic moment vector of dipole i by $\boldsymbol{m}_i$ and assume that it is associated with an angular momentum $\boldsymbol{L}_i$ according to the standard formula

$$\boldsymbol{m}_i = \gamma\, \boldsymbol{L}_i\ , \quad i = 1, 2\ , \tag{1}$$

where γ is the gyromagnetic ratio

$$\gamma = -\frac{e_0}{2m_e} g\ , \tag{2}$$

independent of i. γ is assumed to be negative due to the negative charge $-e_0$ of the electron (m_e denoting its mass) and the gyromagnetic factor g is considered as a physical property of the dipoles. We expect that g varies between $g = 1$ for the contribution due to pure orbital motion of the electrons and $g = 2$ for the spin contribution to the magnetism of the dipoles. Furthermore we will assume that the torque exerted on a dipole by a magnetic field $\boldsymbol{B}$ is equal to

$$\boldsymbol{N} = \boldsymbol{m} \times \boldsymbol{B}\ . \tag{3}$$

This textbook equation is usually derived for systems of moving charges and constant magnetic fields. Hence the validity of (3) for the problem under consideration is not trivial but an additional assumption. In our case there are two magnetic fields, $\boldsymbol{B}_1$ and $\boldsymbol{B}_2$, where $\boldsymbol{B}_2$ denotes the instantaneous value of the magnetic field at $\boldsymbol{m}_1$ due to dipole 2, and an analogous definition applies for $\boldsymbol{B}_1$ due to dipole 1. Thus, for example,

$$\boldsymbol{B}_2 = \frac{\mu_0}{4\pi a^3} \left(3\boldsymbol{m}_2 \cdot \boldsymbol{e}\, \boldsymbol{e} - \boldsymbol{m}_2\right)\ , \tag{4}$$

where $\boldsymbol{e}$ is a unit vector parallel to the constant position vector from dipole 1 to dipole 2. Hence we obtain

$$\frac{d}{dt}\boldsymbol{m}_1 = \gamma\, \frac{d}{dt}\boldsymbol{L}_1 = \gamma\, \boldsymbol{m}_1 \times \boldsymbol{B}_2 = \frac{\gamma\mu_0}{4\pi a^3}\, \boldsymbol{m}_1 \times \left(3\boldsymbol{m}_2 \cdot \boldsymbol{e}\, \boldsymbol{e} - \boldsymbol{m}_2\right)\ . \tag{5}$$

Introducing the unit vectors $\boldsymbol{s}_i = \frac{1}{M}\boldsymbol{m}_i,\ i = 1, 2$ where $M = |\boldsymbol{m}_1| = |\boldsymbol{m}_2|$ is constant, and utilizing (2) we rewrite (5) as

$$\frac{d}{dt}\boldsymbol{s}_1 = -\frac{\mu_0 e_0\, g\, M}{8\,\pi\, m_e\, a^3}\, \boldsymbol{s}_1 \times \left(3\boldsymbol{s}_2 \cdot \boldsymbol{e}\, \boldsymbol{e} - \boldsymbol{s}_2\right) = -\omega_0\, \boldsymbol{s}_1 \times \left(3\boldsymbol{s}_2 \cdot \boldsymbol{e}\, \boldsymbol{e} - \boldsymbol{s}_2\right)\ . \tag{6}$$

Here we have introduced the constant ω_0, with dimension 1/time, defined by

$$\omega_0 \equiv \frac{\mu_0 e_0\, g\, M}{8\,\pi\, m_e\, a^3}\ . \tag{7}$$

Using $\omega_0 t$ as a dimensionless time variable, again denoted by t, and considering the analogous equation of motion (eom) for the second dipole, we eventually obtain the following system of coupled first order differential equations:

$$\frac{d}{dt}\boldsymbol{s}_1 = \ -\ \boldsymbol{s}_1 \times (3\boldsymbol{s}_2 \cdot \boldsymbol{e}\ \boldsymbol{e} - \boldsymbol{s}_2)\ , \tag{8}$$

$$\frac{d}{dt}\boldsymbol{s}_2 = \ -\ \boldsymbol{s}_2 \times (3\boldsymbol{s}_1 \cdot \boldsymbol{e}\ \boldsymbol{e} - \boldsymbol{s}_1)\ . \tag{9}$$

In view of possible applications mentioned in the Introduction we stress that the derivation of the eom (8), (9) is based on the following three idealized assumptions:

- The two dipoles can be assumed as point-like objects,
- the constant ω_0 is small enough such that the quasi-static approximation of the complete set of Maxwell's equations is valid, and
- the magnetic field is weak enough such that diamagnetic effects can be safely neglected.

We will shortly analyze these assumptions in view of possible applications for magnetic nanostructures. If the dipoles are not point-like objects but rather "physical dipoles" described by an extended dipole density two complications may arise. The magnetic field generated by a physical dipole will, in general, not be a pure dipole field but also have higher multipole contributions. Furthermore, the torque exerted upon a physical dipole in a non-constant magnetic field will, in general, no longer be given by the simple formula (3). A general condition that is sufficient to avoid these complications is $d \ll a$, where d denotes a typical diameter of a single nanomagnet. However, for special dipole densities this condition may be relaxed. For example, the magnetic dipole generated by a rotating sphere with a uniform surface charge behaves in both respects mentioned above like a point dipole [19]. In the experiments reported in [2] magnetic islands are placed on a square lattice with $d = a = 150\,nm$, and consequently higher pole interactions have to be considered. A similar situation occurs for the magnetic dimers investigated in [1], where $d = 600\,nm$ and $a = 800, \ldots, 1200\,nm$.

The second assumption can be expressed by an inequality between two times. The time $T_0 = 1/\omega_0$ is the typical time for changes according to the eom (6). It should be large in comparison to the time $T_1 = a/c$ needed by an electromagnetic wave to cross the distance a between the two dipoles; hence the second assumption of a quasi-static regime can be written as $T_0 = 1/\omega_0 \gg a/c = T_1$. For an experimental situation with $a = 100\ nm$, $g = 1$ and $M = 10^3\ \mu_B$ we have $T_0 \approx 1.2 \times 10^{-5}\,s$ and $T_1 \approx 3.3 \times 10^{-16}\,s$, thus $T_0 \gg T_1$ is very well satisfied.

For the same experimental situation a crude estimate shows that the diamagnetic correction δM to the magnetic moment M of a nanomagnet satisfies $\delta M < 10^{-11}\,M$ and hence the third assumption would also be satisfied.

2.2. Solution of the equation of motion

To facilitate solving the eom (8), (9) we first note that these equations give rise to two conserved physical quantities, to be denoted by Q_1 and Q_2:

$$Q_1 = \boldsymbol{S} \cdot \boldsymbol{e} \ , \tag{10}$$

where $\boldsymbol{S} \equiv \boldsymbol{s}_1 + \boldsymbol{s}_2$, and Q_2 is the dimensionless energy

$$Q_2 = H \ , \tag{11}$$

that can be written in any one of the following four forms

$$H = \ - \boldsymbol{s}_1 \cdot (3\boldsymbol{s}_2 \cdot \boldsymbol{e}\ \boldsymbol{e} - \boldsymbol{s}_2) \tag{12}$$

$$= \ - 3\boldsymbol{s}_1 \cdot \boldsymbol{e}\ \boldsymbol{s}_2 \cdot \boldsymbol{e} + \boldsymbol{s}_1 \cdot \boldsymbol{s}_2 \tag{13}$$

$$= \ - \frac{1}{E_0}\boldsymbol{m}_1 \cdot \boldsymbol{B}_2 = -\frac{1}{E_0}\boldsymbol{m}_2 \cdot \boldsymbol{B}_1 \ . \tag{14}$$

Here we have introduced the unit of energy

$$E_0 = \frac{\mu_0\, M^2}{4\pi\, a^3} \ . \tag{15}$$

The quantity Q_1 is proportional to the component of the total magnetic moment in the direction of $\boldsymbol{e}$ and obviously conserved due to the azimuthal symmetry of the problem in the spirit of Noether's theorem. Moreover, from (14) it is clear that Q_2 is proportional to the total energy of the magnetic field originating in the pair of dipoles. Its conservation reflects the time-translational symmetry of the problem.

It can be shown that (12) is the Hamiltonian for the system (8),(9) as well in the sense of classical mechanics. More precisely, we consider (8),(9) as an eom on the 4-dimensional phase space $\mathcal{S}^2 \times \mathcal{S}^2$ with canonical coordinates $(p_i,\, q_i) = (\phi_i,\, z_i)$, $i = 1, 2$ defined by

$$\boldsymbol{s}_i = \begin{pmatrix} \sqrt{1 - z_i^2}\cos\phi_i \\ \sqrt{1 - z_i^2}\sin\phi_i \\ z_i \end{pmatrix} \ , \tag{16}$$

where the z-axis has been chosen in the direction of $\boldsymbol{e}$, and rewrite (8),(9) in the following form:

$$\dot{\phi_1} = \frac{z_1\sqrt{1 - z_2^2}}{\sqrt{1 - z_1^2}}\cos(\phi_1 - \phi_2) + 2z_2 \ , \tag{17}$$

$$\dot{\phi_2} = \frac{z_2\sqrt{1 - z_1^2}}{\sqrt{1 - z_2^2}}\cos(\phi_2 - \phi_1) + 2z_1 \ , \tag{18}$$

$$\dot{z_1} \ = \ \sin(\phi_2 - \phi_1)\sqrt{1 - z_1^2}\sqrt{1 - z_2^2} \ , \tag{19}$$

$$\dot{z_2} \ = \ \sin(\phi_1 - \phi_2)\sqrt{1 - z_2^2}\sqrt{1 - z_1^2} \ , \tag{20}$$

where the dot denotes the derivative w. r. t. time t.

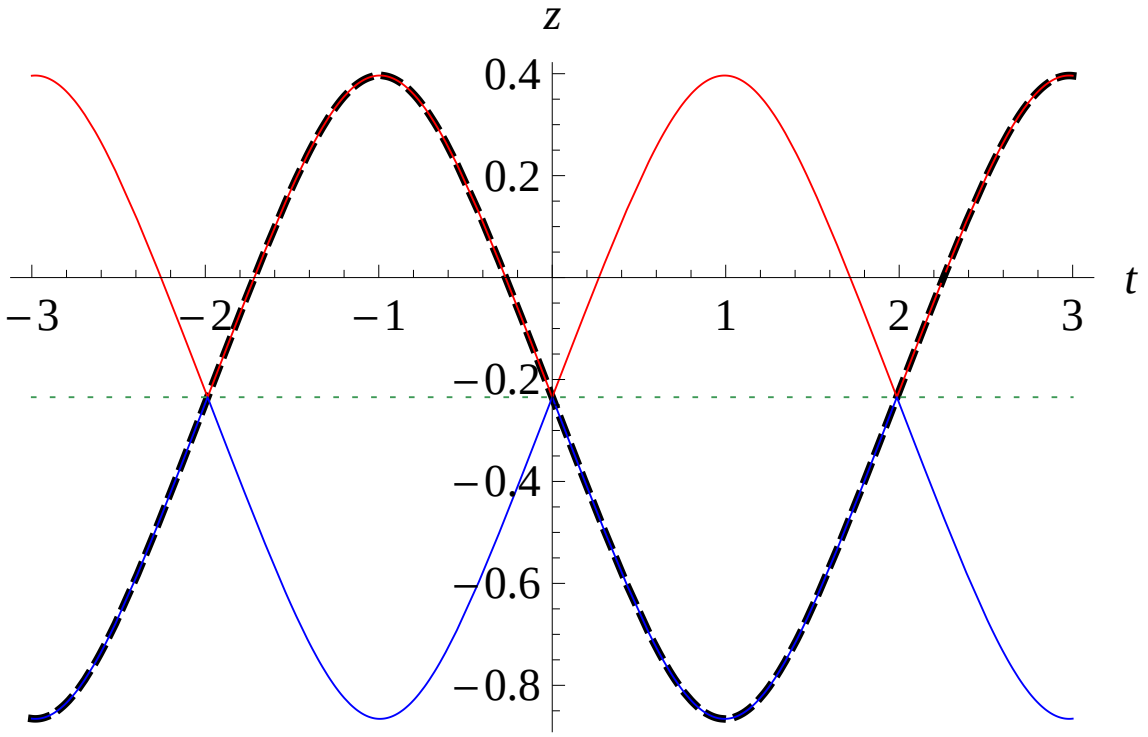

Figure 1. Plot of a periodic solution $z_{1,2}(t)$ of (17)–(20) with randomly chosen initial conditions and period $P = 3.97335$. The solution has been redrawn such that $z_{1,2}(t)$ assumes its mean value (dotted line) at $t = 0$. The black dashed curve represents the numerical solution $z_1(t)$ and the blue/red curves, partially hidden, the analytical solutions (31) according to the sign $\pm$.

As a function of the canonical coordinates H assumes the form

$$H = \sqrt{1 - z_1^2}\sqrt{1 - z_2^2}\cos(\phi_1 - \phi_2) - 2z_1 z_2 \ . \tag{21}$$

Then it follows that

$$\dot{\phi}_i = -\frac{\partial H}{\partial z_i} \ , i = 1, 2 \ , \tag{22}$$

$$\dot{z}_i = \frac{\partial H}{\partial \phi_i} \ , i = 1, 2 \ . \tag{23}$$

Still another way to derive the eom would be to consider the Hamiltonian $\hat{H} = E_0 H$, where the unit vectors $\boldsymbol{s}_i$ are replaced by self-adjoint operators $\hat{\boldsymbol{s}}_i = \frac{\gamma}{M}\hat{\boldsymbol{L}}_i$ $i = 1, 2$ and the $\hat{\boldsymbol{L}}_i$ satisfy the usual commutation relation of angular momentum operators, i. e. , $[\hat{L}_x, \hat{L}_y] = i\hbar\hat{L}_z$, etc. Then it follows in the Heisenberg picture that

$$\frac{d}{dt}\hat{\boldsymbol{s}}_1 = \frac{i}{\hbar}[\hat{H}, \hat{\boldsymbol{s}}_1] = -\omega_0\, \hat{\boldsymbol{s}}_1 \times (3\hat{\boldsymbol{s}}_2 \cdot \boldsymbol{e}\, \boldsymbol{e} - \hat{\boldsymbol{s}}_2) \ , \tag{24}$$

and analogously for $\frac{d}{dt}\hat{\boldsymbol{s}}_2$. The classical limit of (24) is equivalent to (8) if the dimensionless time variable is introduced.

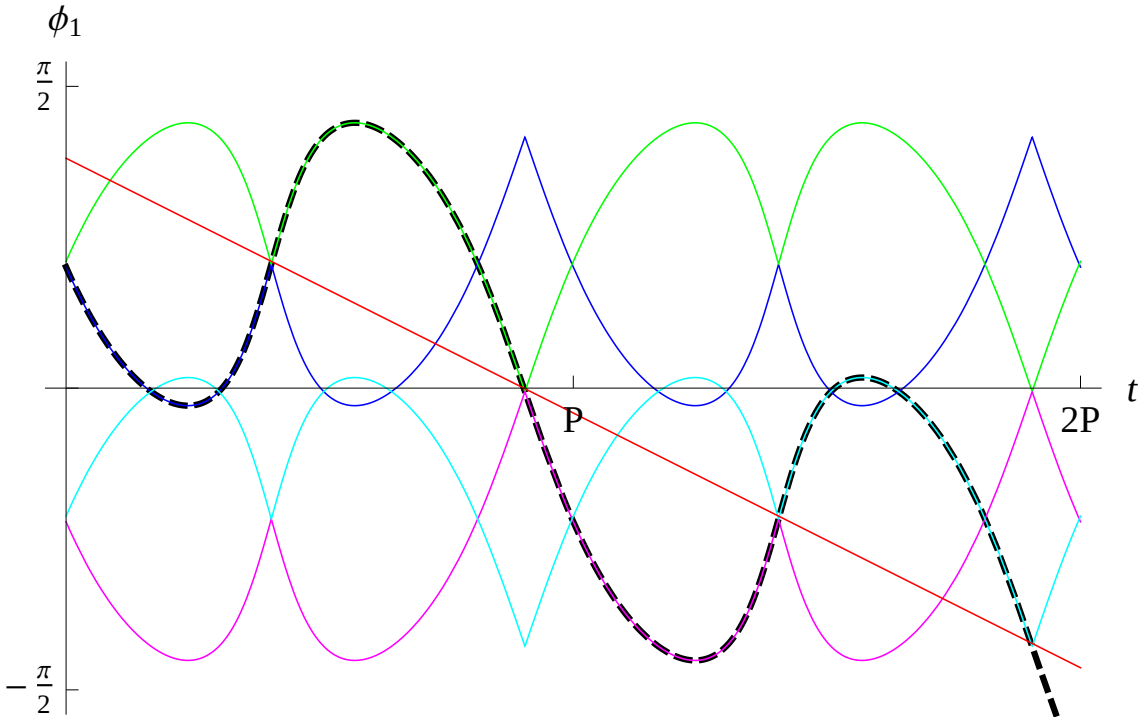

Figure 2. Plot of a numerical solution $\phi_1(t)$ of (17)–(20) with the same initial conditions as in figure 1 (black dashed line). One notes a constant drift (red line) superimposed by a periodic oscillation with the same period P as for $z_{1,2}(t)$. We have also displayed a couple of functions of the form (C.13) that piecewise represent analytical solutions $\phi_1(t)$.

It can be shown that the solution $(\phi_1(t), z_1(t), \phi_2(t), z_2(t))$ of (17)-(20) moves on a 2-dimensional torus defined by the equations $\boldsymbol{S}\cdot\boldsymbol{e} = \sigma$ and $H = \varepsilon$. Since the number of conserved quantities is half the phase space dimension the system (22), (23) is *completely integrable* in the sense of the Arnol'd–Liouville theorem [21] and its solution can be implicitly expressed in terms of integrals. In our case, these integrals are of elliptic kind and hence the solution can be explicitly given by means of Weierstrass elliptic functions $\mathcal{P}$ and elliptic integrals, see [28] Ch. 17 and 18. We will give some more details of these calculations in Appendix B as well as a short introduction to the theory of elliptic integrals and functions in Appendix A. Here we will immediately formulate the final result for $z_{1,2}(t)$ after defining the quantities

$$g_2 \equiv \frac{4}{27}\left(112\varepsilon^2 + 16\varepsilon\left(3\sigma^2 - 16\right) + 9\sigma^4 - 168\sigma^2 + 208\right), \tag{25}$$

$$g_3 \equiv \frac{8}{729}\left(8\varepsilon + 3\sigma^2 - 4\right) \times \left(80\varepsilon^2 - 48\varepsilon\sigma^2 - 512\varepsilon - 9\sigma^4 - 408\sigma^2 + 560\right), \tag{26}$$

$$v_\pm \equiv \frac{1}{\pm 4\sqrt{(\varepsilon-2)^2 - 3\sigma^2} - 8\varepsilon - 3\sigma^2 + 4}, \tag{27}$$

$$u_2 \equiv -\sqrt{3v_+}\,K\left(8\sqrt{(\varepsilon-2)^2-3\sigma^2}\,v_+\right)\,, \tag{28}$$

$$\mathcal{P}(z) \equiv \mathcal{P}(z;g_2,g_3)\,, \tag{29}$$

$$P = 8\sqrt{v_+}K\left(\frac{v_+}{v_-}\right)\,, \tag{30}$$

$$z_{1,2}(t) = \frac{1}{2}\left(\sigma \pm \sqrt{\mathcal{P}\left(\frac{it\sqrt{3}}{2}+u_2\right)-\mathcal{P}(u_2)}\right)\,. \tag{31}$$

K denotes the complete elliptic integral of first kind, see [28] Ch. 17. The sign $\pm$ in (31) has to be chosen to fit with $z_{1,2}(t)$ according to the initial conditions. $z_{1,2}(t)$ performs periodic oscillations about its mean value $\frac{\sigma}{2}$ with period P according to (30), see figure 1.

We now turn to the solution for $\phi_1(t)$. The conserved quantities (10), (11) can be used to express $\dot{\phi}_1$ solely in terms of z_1:

$$\dot{\phi}_1 = \frac{(\varepsilon-2)z_1+2\sigma}{z_1^2-1}\,. \tag{32}$$

Since $z_1(t)$ is a periodic function, $\phi_1(t)$ will also be periodic in time, except for a constant drift that moves $\phi_1(t)$ with a certain amount δ during one period P. This is illustrated in figure 2. Moreover, it turns out that $\frac{d\phi_1}{dz_1}$ can be written as a function of z_1 that is the quotient of a rational function and a square root of a polynomial of 4th degree. Hence $\phi_1(z_1)$ is expressible in terms of elliptic integrals and, after inserting $z_1(t)$, an explicit form of $\phi_1(t)$ is possible, analogously for $\phi_2(t)$. We defer the details and the final result to Appendix C.

2.3. Action and angle variables

It is well-known [21] that the invariant tori of an $2n$-dimensional completely integrable system can be described by special coordinates $(J_i,\ \psi_i),\quad i=1,\ldots,n$ called *action and angle variables*, such that the eom assume the simple form

$$\frac{d}{dt}J_i = 0,\quad \frac{d}{dt}\psi_i = \Omega_i(J_1,\ldots,J_n),\quad i=1,\ldots,n\,. \tag{33}$$

Moreover, the rotations according to the angles ψ_i are uniquely composed of the phase flows generated by the conserved quantities. In our case of $n=2$ the two conserved quantities $\boldsymbol{J}\cdot\boldsymbol{e}$ and H generate simultaneous rotations of both magnetic moments about the z-axis and time evolution. This implies that the first angle variable ψ_1 can be directly identified, e. g. , with the azimuthal angle of the total moment $\boldsymbol{S}=\boldsymbol{s}_1+\boldsymbol{s}_2$. For ψ_2 the situation is a bit more complicated. The time evolution for one period P restores the initial values of $z_1,\ z_2$ but generates a drift δ of the azimuthal angles $\phi_1,\ \phi_2$, see section 2.2. Hence the rotation according to ψ_2 has to be chosen as the time evolution accompanied by a uniform rotation about the z-axis that exactly compensates the drift. Only then a 2π-rotation of ψ_2 results in the identity transformation of the torus. Consequently, the eom (33) are satisfied with

$$\Omega_1 = \frac{\delta}{P},\quad \Omega_2 = \frac{2\pi}{P}\,. \tag{34}$$

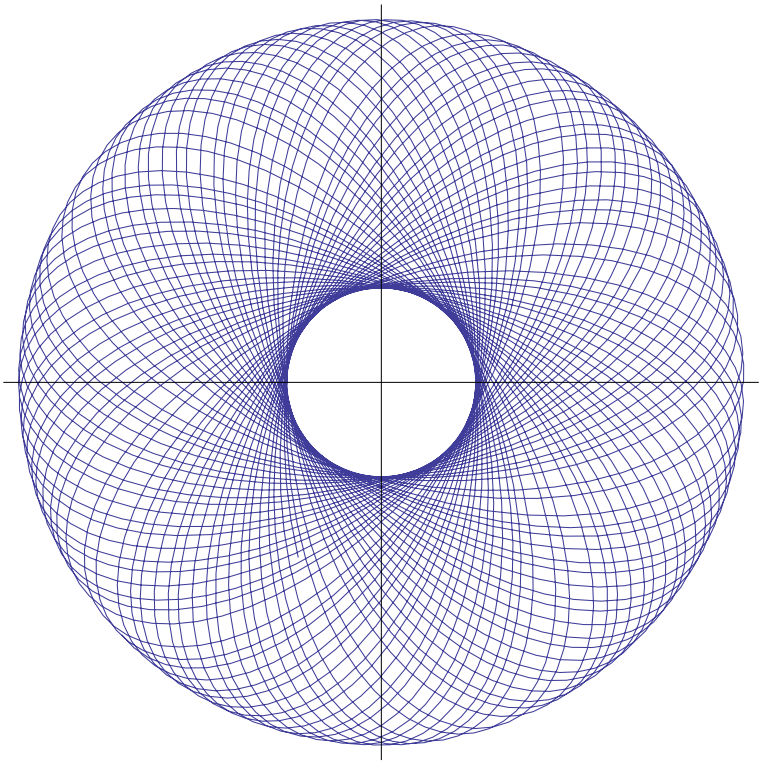

Figure 3. Parametric plot of the total magnetic moment $(\boldsymbol{S}_1(t), \boldsymbol{S}_2(t))$ with the same randomly chosen initial conditions as in figure 1 and $-100 < t < 100$. This solution illustrates the dense filling of the invariant torus defined by $\boldsymbol{J} \cdot \boldsymbol{e} = \sigma$ and $H = \varepsilon$ by the orbit of the system in the case of an irrational ratio $\delta : 2\pi$, where δ is the drift of the azimuthal angles during one period P.

Taking this into account we obtain the following parametric representation of the invariant tori by the angle variables $\psi_1,\ \psi_2 \in [0, 2\pi]$.

$$\boldsymbol{s}_i(\psi_1, \psi_2) = \begin{pmatrix} \sqrt{1 - z_i^2(t_2)}\cos\left(\phi_i(t_2) - \Omega_1 t_2 + \psi_1\right) \\ \sqrt{1 - z_i^2(t_2)}\sin\left(\phi_i(t_2) - \Omega_1 t_2 + \psi_1\right) \\ z_i(t_2) \end{pmatrix}, \quad i = 1, 2, \tag{35}$$

using the abbreviation

$$t_2 \equiv \frac{P}{2\pi}\psi_2 \ . \tag{36}$$

Note that the values of $\boldsymbol{S} \cdot \boldsymbol{e} = \sigma$ and $H = \varepsilon$ characterizing the torus are obtained by the initial values of the solution $z_i(t), \phi_i(t),\ i = 1, 2$ of the eom that occurs in the equation (35).

Obviously, $J_1 = \boldsymbol{S} \cdot \boldsymbol{e}$. It would also be possible to calculate the action variable J_2 by the methods used in the Appendix C. We leave this task to the reader since the result will not be used in the present paper. Rather we will add the following remarks about the ergodicity of our system.

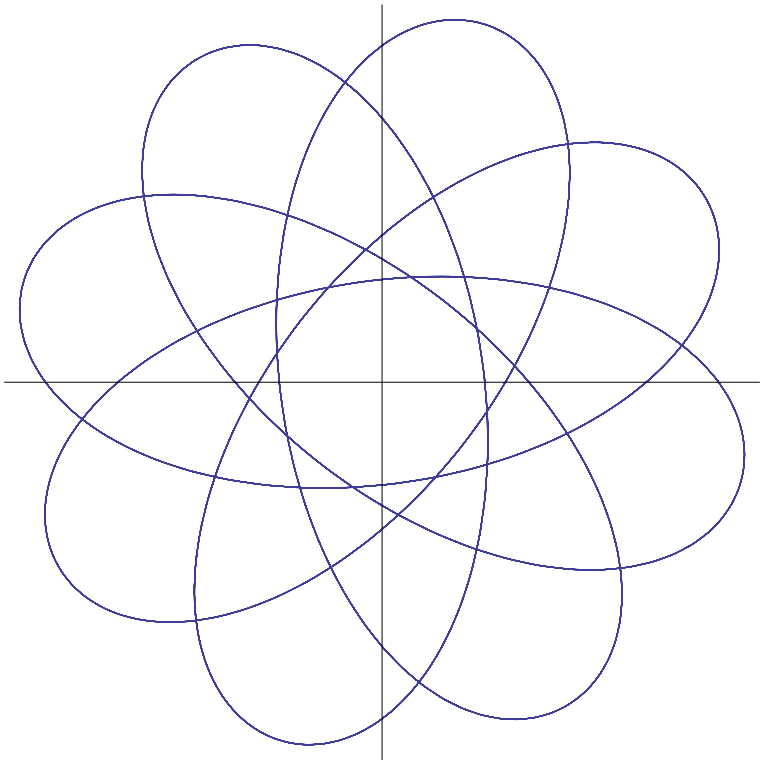

Figure 4. Parametric plot analogous to that of figure 3 of a periodic solution $(\boldsymbol{S}_1(t), \boldsymbol{S}_2(t))$ for $-100 < t < 100$, where the initial conditions have been chosen such that the ratio $\delta : 2\pi$ assumes the value $\frac{1}{8}$.

Surely the system is not ergodic in the usual sense since its orbits are confined to the invariant tori and do not densely fill the whole energy surface $H = \varepsilon$. However, one may ask whether the system is ergodic in the modified sense that the time average of observables equals the average over the particular torus the system is confined to. Here the answer depends on whether the ratio of the angular frequencies $\Omega_1 : \Omega_2 = \delta : 2\pi$ is rational or irrational. Only in the latter case the orbit densely fills the torus and the system is ergodic in the above sense. In order to illustrate this distinction we have displayed the projection of $\boldsymbol{S}(t) = \boldsymbol{s}_1(t) + \boldsymbol{s}_2(t)$ onto the plane perpendicular to $\boldsymbol{e}$ (i. e. the $x - y$-plane) for both cases, see the figures 3 and 4. The case of a rational $\delta : 2\pi$ is interesting in its own right since it yields periodic solutions of the eom but it will only occur for a set of initial values of measure 0.

2.4. Solutions close to the ground states

The configuration $(\boldsymbol{s}_1, \boldsymbol{s}_2)$ with minimal energy (12) under the constraints $|\boldsymbol{s}_1|^2 = |\boldsymbol{s}_2|^2 = 1$ is a *critical point* of (12), i. e. , it satisfies the conditions

$$-\nabla_{\boldsymbol{s}_1} H = 3\, \boldsymbol{s}_2 \cdot \boldsymbol{e}\, \boldsymbol{e} - \boldsymbol{s}_2 = \lambda_1\, \boldsymbol{s}_1 \,, \tag{37}$$

$$-\nabla_{\boldsymbol{s}_2} H = 3\, \boldsymbol{s}_1 \cdot \boldsymbol{e}\, \boldsymbol{e} - \boldsymbol{s}_1 = \lambda_2\, \boldsymbol{s}_2 \,, \tag{38}$$

where $\lambda_1,\ \lambda_2$ are Lagrange parameters due to the constraints. Upon forming the scalar product of both equations with $\boldsymbol{e}$ one easily derives the following alternative: Either $\boldsymbol{s}_1\cdot\boldsymbol{e}=\boldsymbol{s}_2\cdot\boldsymbol{e}=0$ or $\lambda_1\lambda_2=4$ and $\boldsymbol{s}_i=\pm\,\boldsymbol{e},\ i=1,2$. In the first case, $H=\boldsymbol{s}_1\cdot\boldsymbol{s}_2\geq -1$, whereas in the second case the function H assumes the ground state energy $\varepsilon_0=-2$ if $\boldsymbol{s}_1=\boldsymbol{s}_2=\pm\boldsymbol{e}$. Hence the two ferromagnetic configurations parallel to $\boldsymbol{e}$ constitute the ground states of the dipole pair.

The energy barrier between the two ground states has the value $\Delta E=1$. This can be seen as follows. Any path π in phase space joining the two ground states has at least one local energy maximum of height $h(\pi)$. The minimum ε_1 of $h(\pi)$ among all such paths π is necessarily assumed at a saddle point and hence at a critical point of (12). From the above classification of critical points only the possibilities $\boldsymbol{s}_1\cdot\boldsymbol{e}=\boldsymbol{s}_2\cdot\boldsymbol{e}=0$ remain as candidates for saddle points and in this set only the configurations with $\boldsymbol{s}_1=-\boldsymbol{s}_2$ assume the minimal energy $\varepsilon_1=-1$. Hence $\Delta E=\varepsilon_1-\varepsilon_0=1$.

For energies slightly above $\varepsilon_0=-2$ it is sensible to linearize the eom. Writing

$$\boldsymbol{s}_1=\begin{pmatrix}X_1\\X_2\\-1\end{pmatrix}+\mathcal{O}(|\boldsymbol{X}|^2)\ ,\quad \boldsymbol{s}_2=\begin{pmatrix}X_3\\X_4\\-1\end{pmatrix}+\mathcal{O}(|\boldsymbol{X}|^2)\ , \tag{39}$$

we obtain the linearized eom in the form

$$\dot{\boldsymbol{X}}(t)=\boldsymbol{A}\ \boldsymbol{X}(t)\ , \tag{40}$$

where $\boldsymbol{X}=(X_1,X_2,X_3,X_4)$. The matrix $\boldsymbol{A}$ has the form

$$\boldsymbol{A}=\begin{pmatrix}0&2&0&1\\-2&0&-1&0\\0&1&0&2\\-1&0&-2&0\end{pmatrix}\ , \tag{41}$$

and its eigenvalues are $\pm i,\pm 3i$. For later purposes we write down the first two components of the solutions of (40) using the initial conditions $X_i(0)=x_i,\ i=1,\ldots,4$.

$$\begin{aligned}X_1(t)=\frac{1}{2}\,&((x_1-x_3)\cos(t)+(x_2-x_4)\sin(t)+\\&(x_1+x_3)\cos(3t)+(x_2+x_4)\sin(3t))\ ,\end{aligned} \tag{42}$$

$$\begin{aligned}X_2(t)=\frac{1}{2}\,&((x_2-x_4)\cos(t)+(x_3-x_1)\sin(t)+\\&(x_2+x_4)\cos(3t)-(x_1+x_3)\sin(3t))\ .\end{aligned} \tag{43}$$

From this we can calculate the lowest non-trivial order of

$$z_1(t)=\ \pm\ \sqrt{1-(X_1(t)^2+X_2(t)^2)} \tag{44}$$

$$=\ -1+\frac{1}{2}(X_1(t)^2+X_2(t)^2)+\mathcal{O}(|\boldsymbol{X}|^4) \tag{45}$$

$$=\ -1+\frac{1}{4}\Big((x_1^2+x_2^2+x_3^2+x_4^2)+$$

$$+\left(x_1^2+x_2^2-x_3^2-x_4^2\right)\cos(2t)+2\left(x_1x_4-x_2x_3\right)\sin(2t))+\mathcal{O}(|\boldsymbol{X}|^4)\ . \tag{46}$$

At first sight it is remarkable that $z_1(t)$ contains no term proportional to $\sin(6t)$ or $\cos(6t)$ as one would expect from the possible addition of frequencies in $X_1(t)^2+X_2(t)^2$. However, the result (46) is in accordance with the low energy limit of the exact solution (29) of $z_1(t)$. Hence in the low energy limit $\boldsymbol{s}_1(t)$ performs a harmonic oscillation with the two angular frequencies $\omega_1=1$ and $\omega_2=3$ in the $x-y-$plane and $\omega_3=2$ in the $z-$direction. Recall that according to (7) we have chosen the unit of angular frequency to be ω_0.

3. Thermodynamics

A direct experimental test of the results of section 2 for nanomagnets is naturally affected by thermal fluctuations due to finite temperatures. Hence it seems worth while to investigate the thermodynamics of magnetic dipoles, especially to calculate thermodynamic functions such as the specific heat and the susceptibility. Furthermore, we will consider the autocorrelation function (acf) in the low temperature limit. The theoretical results will be compared with those of simulations of the system of two magnetic dipoles coupled to a heat bath. The methods used are described in the following subsection.

A few words are in order concerning the choice of the statistical ensemble that is used to calculate the thermodynamical functions. It has been argued [22] that the microcanonical and the canonical (Gibbs) ensemble are not equivalent for systems of magnetic dipoles due to the long range character of their interaction. This applies all the more to the system under consideration since we have $N=2$ and thus are far from the thermodynamic limit. Assuming the positions of the two dipoles as fixed, our system cannot be considered as isolated. The experimental situation we have in mind consists of nanomagnets embedded into a matrix that constitutes a kind of heat bath. Hence the canonical ensemble seems to be the natural choice and we have performed the subsequent calculations in this framework. Nevertheless, the comparison of our results with calculations in the microcanonical ensemble might be interesting since the statistical mechanics of integrable systems is an actual field of research, see, e. g. , [23]. However, such a comparison is outside the scope of the present paper.

3.1. Methods

As it is well-known, thermodynamic functions such as the free energy and the specific heat can be derived from the partition function $Z(\beta)$ of the system. We will present below an explicit form of $Z(\beta)$ for the Hamiltonian (11), based on the determination of the density of states function (dos) $\rho(\varepsilon)$. Hence we could give an explicit formula for the specific heat albeit a very intricate one. For the calculation of the specific heat $c(T)$ as a

function of (dimensionless) temperature T we rather resort to the numerical evaluation of the integral representation since the special functions occurring in the explicit form of $Z(\beta)$ are not implemented in the computer algebra software we used.

For the calculation of the susceptibility we need not only $Z(\beta)$ but also certain moments (72), (77) of the total magnetic dipole moment $\boldsymbol{S}$. The method used for the specific heat cannot be generalized to the calculation of the susceptibility, since it would involve a generalized dos $\rho(\varepsilon, \sigma)$ that is not known. Fortunately, there exist powerful approximation schemes to overcome this difficulty. On the one hand it is possible to explicitly derive all moments of H and thus the complete high temperature expansion (HTE) series of $Z(\beta)$. On the other hand, the integrals over the 4-dimensional phase space defining $Z(\beta)$ can be transformed conveniently to allow for a low temperature asymptotic expansion (LTA) of several orders of, say, $n = 12$. We will sketch the method of asymptotic evaluation of phase space integrals below although the LTA of the partition function can also be directly obtained by the Taylor expansion of the dos at $\varepsilon = \varepsilon_0$. However, this method can be extended to obtain the LTA of the zero field susceptibility $\chi(\beta)$ for both axes. Moreover, the moments needed for the HTE of the susceptibilities can be determined similarly as for $Z(\beta)$. Since the easy axis susceptibility $\chi(T)$ diverges for $T \to 0$ with the power T^{-1} it is more appropriate to plot the product $T\ \chi(T)$ as a function of T. In contrast to this, the hard axis susceptibility approaches a finite value for $T \to 0$.

The investigation of the autocorrelation function acf and its thermal average $\langle \mathrm{acf} \rangle$ combines dynamical and thermodynamical aspects of the system under consideration. As mentioned above, we will restrict ourselves to the low temperature asymptotic expansion up to terms of first order in T. In this realm it is sufficient to consider the solutions of the eom close to the ground states, see subsection 2.4, and to perform the integrations within the "harmonic oscillator approximation", i. e. an approximation of the Hamiltonian that is quadratic in the deviations from the ground state. However, for long times this approximation breaks down and we observe a relaxation of $\langle \mathrm{acf} \rangle$ to constant values that are identical with the mean values of the initial oscillation, see subsection 3.6.2. Furthermore, we have used classical spin dynamics and Monte Carlo simulations in order to compare our analytical derivations with numerical results.

3.2. Density of states

It is possible to analytically calculate the density of state (dos) function $\rho(\varepsilon)$, where $-2 \leq \varepsilon \leq 2$ denotes the dimensionless energy of the dipole pair. We will only sketch the main ideas of the derivation. Obviously, $\rho(\varepsilon)$ is a symmetric function since the transformation $(\boldsymbol{s}_1, \boldsymbol{s}_2)) \mapsto (\boldsymbol{s}_1, -\boldsymbol{s}_2))$ leaves the phase space volume invariant, but inverts the sign of the energy. Hence it suffices to calculate $\rho(\varepsilon)$ for, say, $-2 \leq \varepsilon \leq 0$.

If the first moment $\boldsymbol{s}_1$ is kept fixed the set of $\boldsymbol{s}_2$ such that $H(\boldsymbol{s}_1, \boldsymbol{s}_2) \leq \varepsilon$ forms a

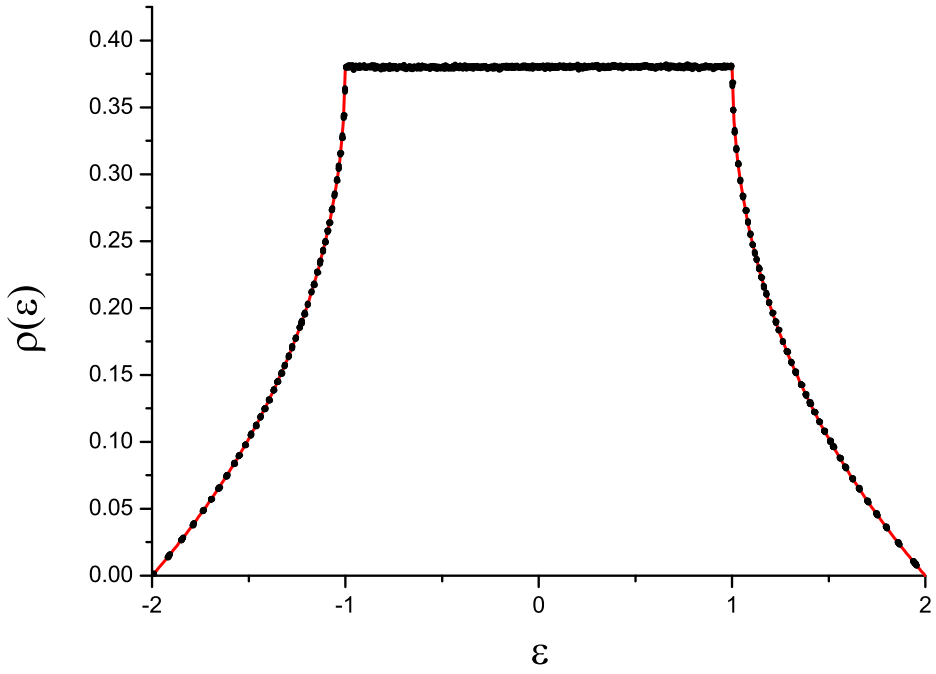

Figure 5. Plot of the density of states $\rho(\varepsilon)$ for the dipole pair obtained by Wang-Landau-sampling together with the analytical result (50) (red curve). It is remarkable that $\rho(\varepsilon)$ assumes the constant value $\frac{\sinh^{-1}(\sqrt{3})}{2\sqrt{3}} \approx 0.380173$ in the interval $-1 \leq \varepsilon \leq 1$.

spherical segment. This segment has the area

$$A(z_1) = 2\pi \left(1 + \frac{\varepsilon}{\sqrt{1+3z_1^2}}\right) . \tag{47}$$

There is a marked difference between the energy domains $-2 \leq \varepsilon \leq -1$ and $-1 \leq \varepsilon \leq 0$: In the latter domain the above spherical segment is always non-empty, whereas for $-2 \leq \varepsilon \leq -1$ and $|z_1| < z(\varepsilon) \equiv \frac{\sqrt{\varepsilon^2-1}}{\sqrt{3}}$ it is empty. We set $z(\varepsilon) = 0$ in the first case and obtain for the integrated dos written as a function $\Phi(\varepsilon)$:

$$\Phi(\varepsilon) = \int_{z(\varepsilon)}^{1} \frac{1}{4\pi} A(z_1)\, dz_1 \tag{48}$$

$$= \begin{cases} \frac{1}{2\sqrt{3}} \left(-\sqrt{\epsilon^2-1} + \epsilon \sinh^{-1}\left(\sqrt{\epsilon^2-1}\right) + \epsilon \sinh^{-1}\left(\sqrt{3}\right) + \sqrt{3}\right) & : \ -2 \leq \varepsilon \leq -1 \\ \frac{1}{2\sqrt{3}} \left(\epsilon \sinh^{-1}\left(\sqrt{3}\right) + \sqrt{3}\right) & : \ -1 \leq \varepsilon \leq 0. \end{cases} \tag{49}$$

From this we obtain the dos

$$\rho(\varepsilon) = \frac{d}{d\varepsilon}\Phi(\varepsilon) = \begin{cases} \frac{1}{2\sqrt{3}} \left(\sinh^{-1}\left(\sqrt{3}\right) - \sinh^{-1}\left(\sqrt{\varepsilon^2-1}\right)\right) & : \ -2 \leq \varepsilon \leq -1 \\ \frac{1}{2\sqrt{3}} \left(\sinh^{-1}\left(\sqrt{3}\right)\right) & : \ -1 \leq \varepsilon \leq 0. \end{cases} \tag{50}$$

The analytical result (50) coincides with the numerical result of the dos determined by Wang-Landau-sampling [24], see figure 5.

3.3. Partition function

3.3.1. Explicit form The partition function $Z(\beta)$ is related to the dos $\rho(\varepsilon)$ by the following formula

$$Z(\beta) = \int_{-2}^{2} \rho(\varepsilon)\, \exp(-\beta\varepsilon)\, d\varepsilon \ , \tag{51}$$

that represents essentially a Laplace transformation. Here β is the dimensionless inverse temperature

$$\beta = \frac{E_0}{k_B T} \ , \tag{52}$$

where the energy unit E_0 has been defined in (12). We will also use the dimensionless temperature $\frac{k_B T}{E_0}$ which again will be denoted by T without danger of confusion.
It follows immediately that $Z(\beta)$ is an even function since $\rho(\varepsilon)$ is even. The integral (51) with the dos (50) can be solved in closed form if we invoke the theory of *incomplete Bessel functions*. We will stick to the definitions and notation presented in [25]. Hence

$$K_\nu(z, w) = \int_w^\infty e^{-z\, \cosh\, t}\, \cosh \nu t\, dt \ , \tag{53}$$

such that $K_\nu(z, 0) \equiv K_\nu(z)$ is identical to the usual *modified Bessel function*, see [28], 9.6.24.
Substituting (50) into (51), noting that $\rho(\varepsilon)$ is an even function and exploiting the identity $\sinh^{-1} w = \ln(w + \sqrt{w^2 + 1})$, one obtains the result

$$Z(\beta) = \frac{2\rho(1)\sinh(2\beta)}{\beta} - \frac{1}{\sqrt{3}} \int_1^2 \ln(\sqrt{\varepsilon^2 - 1} + \varepsilon)\, \cosh(\beta\varepsilon)\, d\varepsilon \tag{54}$$

$$= \frac{1}{\sqrt{3}} \int_1^2 \frac{\varepsilon}{\sqrt{\varepsilon^2 - 1}}\, \frac{\sinh(\beta\varepsilon)}{\beta\varepsilon}\, d\varepsilon \ , \tag{55}$$

where the last step involves an integration by parts. Note that the integral form (55) of $Z(\beta)$ avoids the case distinction in the definition (50) of $\rho(\varepsilon)$. Further, the substitution $\varepsilon = \cosh t$ casts the integral into the form of (53):

$$Z(\beta) = \frac{1}{\beta\sqrt{3}} \int_0^c \sinh\left(\beta\, \cosh t\right)\, d\varepsilon \tag{56}$$

$$= \frac{1}{2\beta\sqrt{3}} \left(\int_0^c \exp\left(\beta\, \cosh t\right)\, d\varepsilon - \int_0^c \exp\left(-\beta\, \cosh t\right)\, d\varepsilon \right) \tag{57}$$

$$= \frac{1}{2\beta\sqrt{3}} \left(K_0(\beta, c) - K_0(\beta) - K_0(-\beta, c) + K_0(-\beta) \right) \ , \tag{58}$$

where we have set $c \equiv \sinh^{-1}\sqrt{3} = \cosh^{-1} 2$. We note that for the negative first argument $-\beta$ of the incomplete Bessel function the integral representation (53) no longer holds but has to be replaced by an analytic continuation, see [25], similar as for $K_\nu(-\beta)$.
This concludes the calculation of the partition function in closed form. Unfortunately, the incomplete Bessel functions are not implemented in MATHEMATICA 9.0 and hence have to be evaluated by numerical integration.

3.3.2. LTA We now derive the low temperature asymptotic expansion (LTA) of the partition function $Z(\beta)$. According to its definition,

$$Z(\beta) = \frac{1}{(4\pi)^2} \int_{-1}^{1} dz_1 \int_{-1}^{1} dz_2 \int_0^{2\pi} d\phi_1 \int_0^{2\pi} d\phi_2 e^{-\beta H}. \tag{59}$$

For fixed ϕ_2 we substitute $\phi_1 = \phi + \phi_2$ and obtain the partial integral

$$\begin{aligned} \mathcal{I}_1 &\equiv \int_0^{2\pi} d\phi_1 \int_0^{2\pi} d\phi_2 \; e^{-\beta H} \\ &= 2\pi e^{2\beta z_1 z_2} \int_0^{2\pi} d\phi \; e^{-\beta\sqrt{(1-z_1^2)(1-z_2^2)}\cos\phi} \\ &= (2\pi)^2 e^{2\beta z_1 z_2} I_0\left(\beta\sqrt{(1-z_1^2)(1-z_2^2)}\right) \; , \end{aligned} \tag{60}$$

where I_n is the modified Bessel function of nth order. Next we substitute $z_i = -1 + u_i^2,\ u_i \geq 0,\ i = 1, 2$, and obtain

$$\begin{aligned} Z(\beta) = \int_0^{\sqrt{2}} u_1 du_1 \int_0^{\sqrt{2}} u_2 du_2 \exp\left(2\beta(-1+u_1^2)(-1+u_2^2)\right) \\ I_0\left(2\beta u_1 u_2 \sqrt{(1-\frac{1}{2}u_1^2)(1-\frac{1}{2}u_2^2)}\right) \; . \end{aligned} \tag{61}$$

Now we consider the limit $\beta \to \infty$ by introducing polar coordinates $u_1 = \frac{r}{\sqrt{\beta}}\cos\psi,\ u_2 = \frac{r}{\sqrt{\beta}}\sin\psi$, extracting the factor $e^{2\beta}/\beta^2$ and evaluating the remaining integral only in 0th order of its Taylor series in β^{-1}. The domain of integration is extended to the whole first quadrant. This gives the contribution to Z in the limit $\beta \to \infty$ from the neighborhood of the ground state $z_1 = z_2 = -1$. In order to include the equal contribution from the ground state $z_1 = z_2 = 1$ we have to insert a factor 2. We thus obtain the following asymptotic limit

$$Z(\beta) \sim \frac{2\, e^{2\beta}}{\beta^2} \int_0^{\infty} r^3\, e^{-2r^2}\, dr \int_0^{\pi/2} d\psi \frac{1}{2} \sin(2\psi) I_0(r^2 \sin(2\psi)) \tag{62}$$

$$= \frac{2\, e^{2\beta}}{\beta^2} \int_0^{\infty} r^3\, e^{-2r^2} \frac{\sinh(r^2)}{2r^2}\, dr = \frac{e^{2\beta}}{6\beta^2} \; . \tag{63}$$

The method can be extended to obtain the first terms of an asymptotic series expansion for $Z(\beta)$. We omit the details and state the following result:

$$Z(\beta) \sim e^{2\beta}\left(\frac{1}{6\beta^2} + \frac{1}{9\beta^3} + \frac{1}{6\beta^4} + \frac{11}{27\beta^5} + \frac{227}{162\beta^6}\right). \tag{64}$$

This result coincides with the Laplace transform of the first terms of the Taylor expansion of $\rho(\varepsilon)$ at $\varepsilon = -2$ according to (50).

3.3.3. HTE Let us denote by $\mathrm{Tr}(f)$ the integral of a function f over 4-dimensional phase space divided by its volume $(4\pi)^2$ [26]. Then the HTE of $Z(\beta)$ reads

$$Z(\beta) = \mathrm{Tr}\left(e^{-\beta H}\right) = \sum_{n=0}^{\infty} \frac{(-\beta)^n}{n!} \mathrm{Tr}(H^n) \; , \tag{65}$$

where H is the Hamiltonian (12). With the aid of computer algebraic software we calculate the moments $\mathrm{Tr}(H^n)$ and hence the HTE of $Z(\beta)$ with the result

$$Z(\beta) = \sum_{n=0}^{\infty} \frac{4^n \, F\left(1, -n; \frac{1}{2} - n; \frac{1}{4}\right) (-\beta)^{2n}}{(2n+1)^2 (2n)!} \,, \tag{66}$$

where $F(a, b; c; z)$ denotes the hypergeometric function, see [28], Ch. 15. In our case it is a polynomial in z since b is a negative integer. Since $\lim_{n\to\infty} F\left(1, -n; \frac{1}{2} - n; \frac{1}{4}\right) = \frac{4}{3}$ the radius of convergence of (66) is the same as that of the exponential series, namely $r = \infty$. Perhaps this explains the high quality of the approximations schemes based on (66).

The HTE result (66) can also be derived from the integral representation (55) of $Z(\beta)$. Substituting the standard power series expansion

$$\frac{\sinh(\beta\varepsilon)}{\beta\varepsilon} = \sum_{n=0}^{\infty} \frac{(\beta\varepsilon)^{2n}}{(2n+1)!} \tag{67}$$

and performing the integral (55) for each term one obtains

$$Z(\beta) = -\sum_{n=0}^{\infty} \frac{\beta^{2n} \, B_{\frac{1}{4}}(-\frac{1}{2} - n, \frac{1}{2})}{2\sqrt{3}\,(2n+1)!} \,, \tag{68}$$

where $B_z(a, b)$ denotes the *incomplete Beta function*, see [28], 6.6.1. (68) is shown to coincide with (66) by virtue of [28] 6.6.8 and 15.3.3.

3.4. Specific heat

According to the definition of the dimensionless specific heat

$$c(\beta) = \beta^2 \, \frac{\partial^2}{\partial \beta^2} \, \log Z(\beta) \,, \tag{69}$$

we can, in principle, obtain an analytical expression by using the results of the subsection 3.3.1 and the rules for the differentiation of the incomplete Bessel functions, see [25], eq. (4.1). This would require the incomplete Bessel functions $K_1(\beta, c)$ and $K_2(\beta, c)$. We will not present the result since it is rather complicated and a direct evaluation would be cumbersome. Rather we insert the integral representation (51) into (69) and evaluate the resulting integrals numerically. The result is shown in figure 6.

Alternatively, the specific heat can be obtained by numerically calculating the fluctuations of the (dimensionless) total energy ε according to

$$c^*(T) = \frac{1}{T^2} \left(\left\langle \varepsilon^2 \right\rangle - \left\langle \varepsilon \right\rangle^2 \right) \tag{70}$$

by means of Monte Carlo simulations. Both methods yield specific heat functions that agree very closely, see 6.

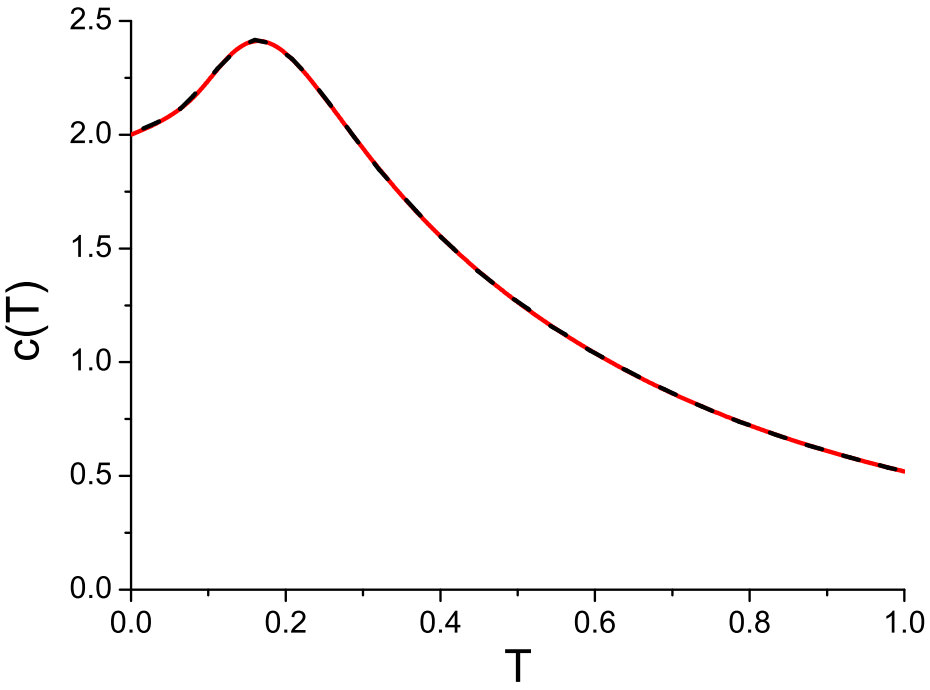

Figure 6. Plot of the specific heat $c(T)$ vs. T. The red curve shows the result of numerically evaluating an integral representation based on the closed form of the density of states function. The black dashed curve shows the results from our Monte Carlo simulation.

3.5. Susceptibility

3.5.1. Easy axis The dimensionless zero field susceptibility for infinitesimal magnetic fields in the direction $\boldsymbol{e}$ joining the two dipoles (the "easy axis") is defined by

$$\chi(\beta) = \beta\langle S_3^2\rangle = \beta\frac{\mathrm{Tr}\,(S_3^2\,\exp(-\beta H))}{Z(\beta)}\ . \tag{71}$$

The HTE of the numerator is

$$\mathrm{Tr}\left(S_3^2\,\exp(-\beta H)\right) = \sum_{n=0}^{\infty}\mathrm{Tr}(S_3^2 H^n)\frac{(-\beta)^n}{n!}\ . \tag{72}$$

Again we can explicitly determine all moments occurring in (72)

$$\mathrm{Tr}(S_3^2 H^m) = \begin{cases} \frac{2^{2n+1}\,F\left(1,-n;-n-\frac{1}{2};\frac{1}{4}\right)}{4n(n+2)+3} & :\quad m=2n, \\ -\frac{2^{2n+1}\left(n\,F\left(1,1-n;\frac{1}{2}-n;\frac{1}{4}\right)+4n+2\right)}{(2n+1)(2n+3)^2} & :\quad m=2n+1, \end{cases} \tag{73}$$

and perform an HTE approximation of $T\chi(T)$ analogously to that of the partition function. The first six terms of this HTE are

$$T\chi(T) = \frac{2}{3} + \frac{4}{9T} + \frac{4}{45T^2} - \frac{16}{675T^3} - \frac{44}{4725T^4} + \frac{352}{99225T^5} + \ldots \tag{74}$$

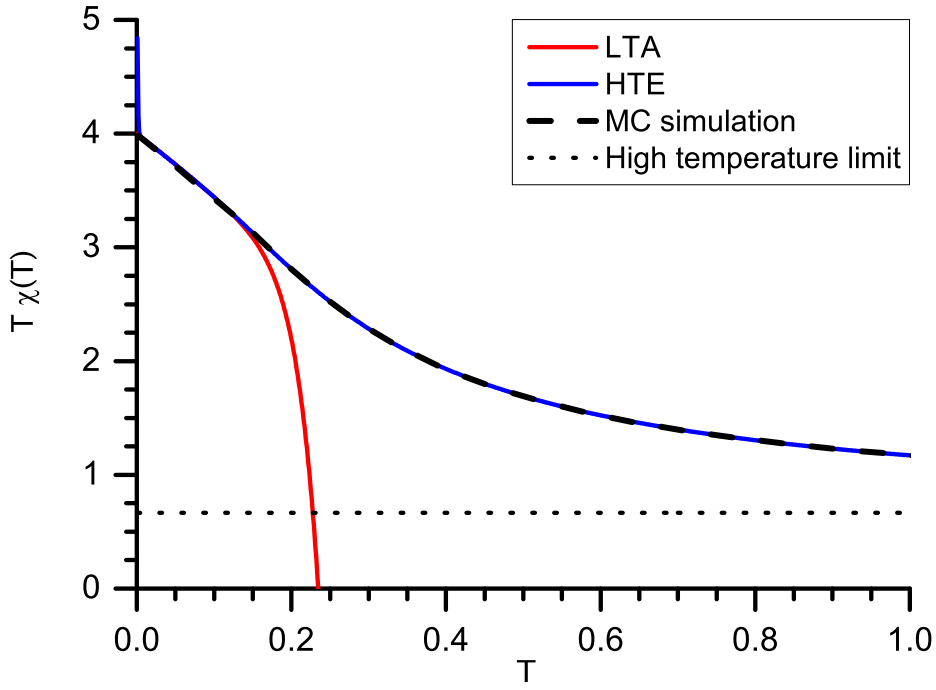

Figure 7. Plot of the product $T\chi(T)$ vs. T for the easy axis. The red curve shows the LTA up to order T^{12}; the blue curve is a $(50, 50)$-Padé approximation based on the HTE of $\chi(\beta)$. Both curves coincide for $0.01 < T < 0.06$ with a maximal relative deviation of 10^{-6}. The black dashed curve shows the results from our Monte Carlo simulation. The dashed line represents the high temperature limit $2/3$ of $T\chi(T)$.

The LTA of $T\chi(T)$ has been calculated up to 12−th order, the first six terms being

$$T\chi(T) = 4 - \frac{16}{3}T - \frac{14}{9}T^2 - \frac{140}{27}T^3 - \frac{1628}{81}T^4 - \frac{23888}{243}T^5 - \dots \tag{75}$$

The combination of HTE and LTA results yields the form of $T\chi(T)$ displayed in figure 7. By means of Monte Carlo simulations, we obtain the dimensionless susceptibility by evaluating the fluctuations of the total magnetization according to

$$\chi^*(T) = \frac{1}{T}\left(\left\langle \boldsymbol{M}^2 \right\rangle - \langle \boldsymbol{M} \rangle^2\right). \tag{76}$$

It is interesting to note that in contrast to the specific heat the susceptibility at very low temperatures cannot be determined correctly by using the standard Metropolis algorithm. As a result of the dipolar interaction an inherent easy-axis anisotropy in the direction of the connecting line between the two dipoles is formed resulting in a bi-stable system. As pointed out in section 2.4 at low temperatures the two dipoles are fluctuating around their two possible ferromagnetic ground states that are separated by an energy barrier of $\Delta E = 1$. During the timescale of a typical computer simulation the two dipoles will be trapped in one of the directions; any attempt to change both dipoles

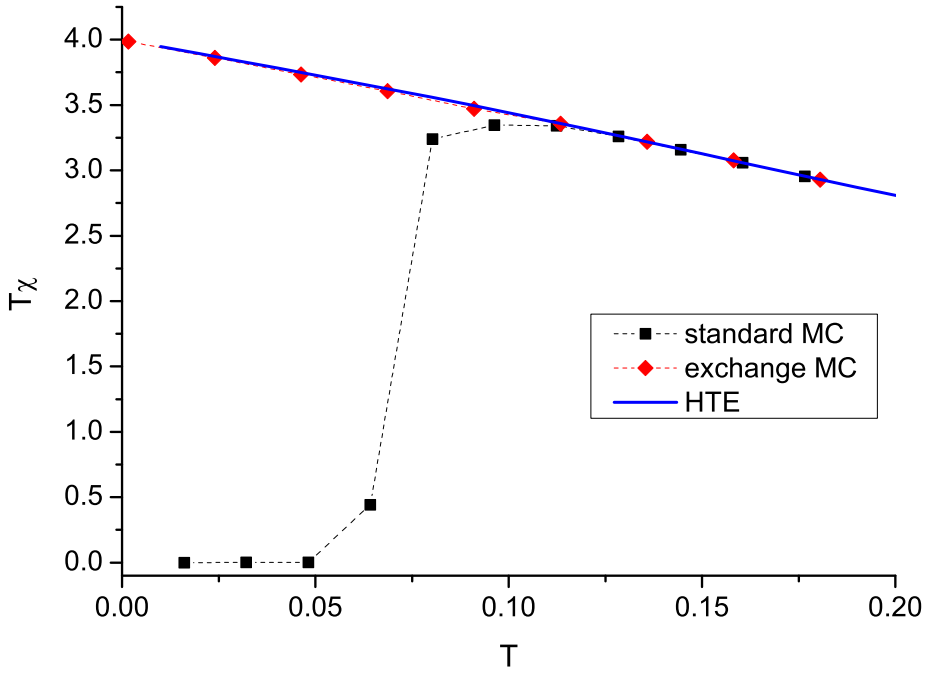

Figure 8. Plot of the product $T\chi(T)$ vs. T for the easy axis. The blue curve shows the Padé approximation based on the HTE of $\chi(\beta)$. For $T < 0.1$ the standard Monte Carlo simulation (black symbols) produces wrong results due to the non-ergodic behavior of the bi-stable dipole system whereas the exchange Monte Carlo method (red symbols) reproduces the analytical results.

from one ground state configuration to the other is rejected in most cases leading to non-ergodic behavior. This is demonstrated in figure 8. In contrast to the analytical results (blue curve) the numerically determined susceptibility drops to zero for temperatures $T < 0.1$.

This can be understood from the following argumentation: According to equation (76) we expect $T\chi \to 4$ for $T \to 0$, because of the z-component of the total magnetization $M_z = 1 + 1$ or $M_z = -1 - 1$ for each of the ground states (M_x and M_y are both zero). This is the variance (fluctuation) of the total magnetization $\mathbf{M}$ since $\langle \mathbf{M} \rangle = 0$ in the ground state. The latter is only valid in a simulation if both ground states are equally often generated such that the average of $\mathbf{M}$ becomes 0. If the system gets trapped in one of the ground states we find $\langle \mathbf{M} \rangle = \pm 2$ and hence the variance vanishes according to $T\chi = 4 - 2 \cdot 2 = 0$.

In order to obtain correct results we have used the so-called Exchange Monte Carlo method [17] in which many replicas of the system with different temperatures are simultaneously simulated and a virtual process exchanging configurations of these replicas is introduced. This exchange process allows the system at low temperatures to

escape from a local minimum and hence producing correct data for the susceptibility (shown as red symbols in figure 8).

Furthermore, it is interesting to note that the specific heat can be obtained correctly by a standard Monte Carlo algorithm. In contrast to the susceptibility which is calculated using the fluctuations of a *directed* property, e. g. the total magnetization, the specific heat is calculated by sampling the fluctuations of the *undirected* total energy. Hence, the low temperature fluctuations in one of the two possible (degenerate) ground states are sufficient to yield the correct statistics.

The same argumentation using the fluctuations of a directed property holds for the simulation of the hard axis susceptibility (see subsection III D 2). However, for this direction there is no energy barrier blocking the system.

3.5.2. Hard axis The zero field susceptibility for the infinitesimal magnetic field in a direction perpendicular to the line joining the two dipoles (the "hard axis") will be calculated by the same methods as for the easy axis. Without loss of generality we choose the x-axis as the hard axis. Again we can explicitly determine all relevant moments

$$\mathrm{Tr}(S_1^2 H^m) = \begin{cases} \frac{2^{2n+1}\left(-(3n+5)\,F\left(1,-n;-n-\frac{1}{2};\frac{1}{4}\right)+4n+6\right)}{4n(n+2)+3} & : m = 2n\,, \\ \frac{9\times 2^{2n+1}\left((3n+5)\,F\left(1,n+\frac{3}{2};n+1;4\right)+n+1\right)\Gamma\left(n+\frac{3}{2}\right)-i\sqrt{3\pi}(3n+5)n!}{18(2n+3)\Gamma\left(n+\frac{5}{2}\right)} & : m = 2n+1, \end{cases} \tag{77}$$

and obtain from this the HTE of the susceptibility and a corresponding $(50, 50)$-Padé approximant that can be used down to low temperatures of, say, $T = 0.01$. The first six terms of this HTE are

$$T\chi(T) = \frac{2}{3} - \frac{2}{9T} - \frac{2}{45T^2} + \frac{26}{675T^3} - \frac{22}{4725T^4} - \frac{626}{99225T^5} + \dots\,. \tag{78}$$

Note that the first term of (78) can be viewed as the Curie constant $C = \frac{2}{3}$ of Curie's law $\chi = \frac{C}{T}$ and coincides with the analogous term of the easy axis susceptibility (74). It is compatible with the high temperature limit

$$\chi(T) = \frac{|\boldsymbol{m}|^2 \mu_0}{3k_B T} \tag{79}$$

of Langevin's formula [18] (5.7) for the susceptibility of a single magnetic dipole, if we consider dimensionless quantities and insert a factor 2 since our result (74), (78) holds for *two* dipoles. The compatibility of (74), (78) and (79) is physically plausible because the interaction between the dipoles is negligible for high temperatures.

The LTA of the hard axis susceptibility leads to the terms

$$\chi(T) = \frac{2}{3} - \frac{2}{9}T - \frac{2}{27}T^2 - \frac{14}{81}T^3 + \mathcal{O}(T^4)\,. \tag{80}$$

Both approximations, HTE and LTA, can be combined and yield a result that is very close to that obtained by Monte Carlo simulations, see figure 9. It is physically plausible

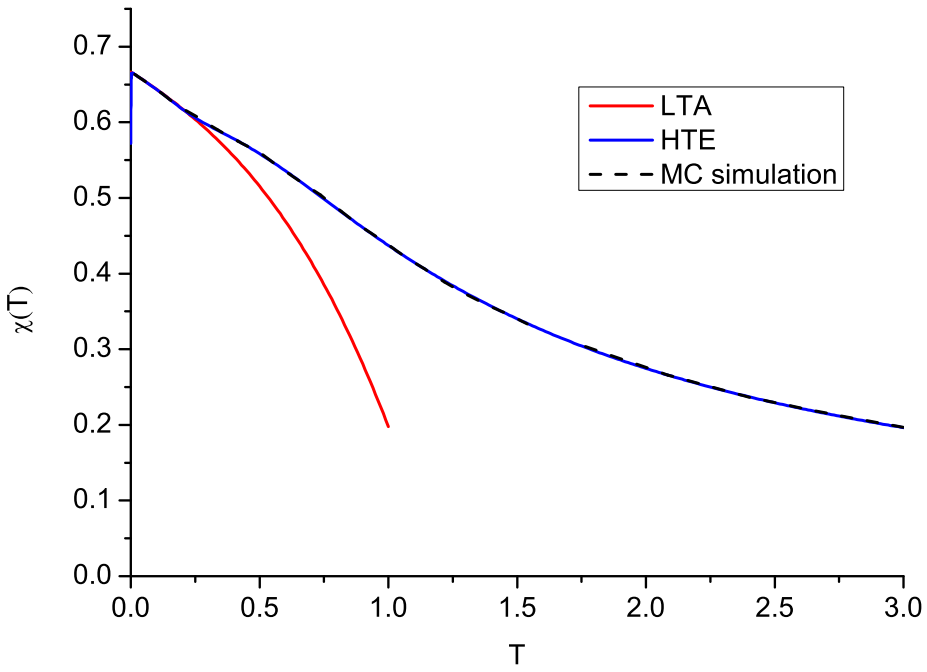

Figure 9. Plot of the hard axis susceptibility $\chi(T)$ vs. T. The blue curve shows the Padé approximation based on the HTE of $\chi(\beta)$, the red curve the LTA according to (80), and the black dashed curve the result of the Monte Carlo simulation.

that a small magnetic field in x-direction only leads to a small additional magnetization relative to that of the ground state. Hence the susceptibility is expected to approach a finite value for $T \to 0$. This is confirmed by the above result for the LTA (80). For the same reason the complications in the Monte Carlo simulations mentioned above, see section 3.5.1, do not occur.

3.6. Autocorrelation function

3.6.1. Short time behavior The autocorrelation function acf or rather its thermal average $\langle \text{acf} \rangle$ provide typical characteristics of a system under the influence of thermal fluctuations. In our case we consider $\text{acf} = \boldsymbol{s}_1(0) \cdot \boldsymbol{s}_1(t)$ (the result for the second dipole would be identical) and will exactly evaluate $\langle \text{acf} \rangle$ in the limit $\beta \to \infty$ for times t comparable with the period P of oscillations (31). From section 2.4 we know already that only the three frequencies $\omega_1 = 1$, $\omega_2 = 3$ and $\omega_3 = 2$ will occur in the Fourier spectrum of low temperature oscillations. Since

$$\text{acf} = \sqrt{(1 - z_1(0)^2)(1 - z_1(t)^2)}\, \cos(\phi_1(0) - \phi_1(t)) + z_1(0) z_1(t)\,, \tag{81}$$

we expect that the contribution $\langle z_1(0) z_1(t) \rangle$ will be suppressed by thermal averaging over all phase shifts of the z_1-oscillations. On the other hand,

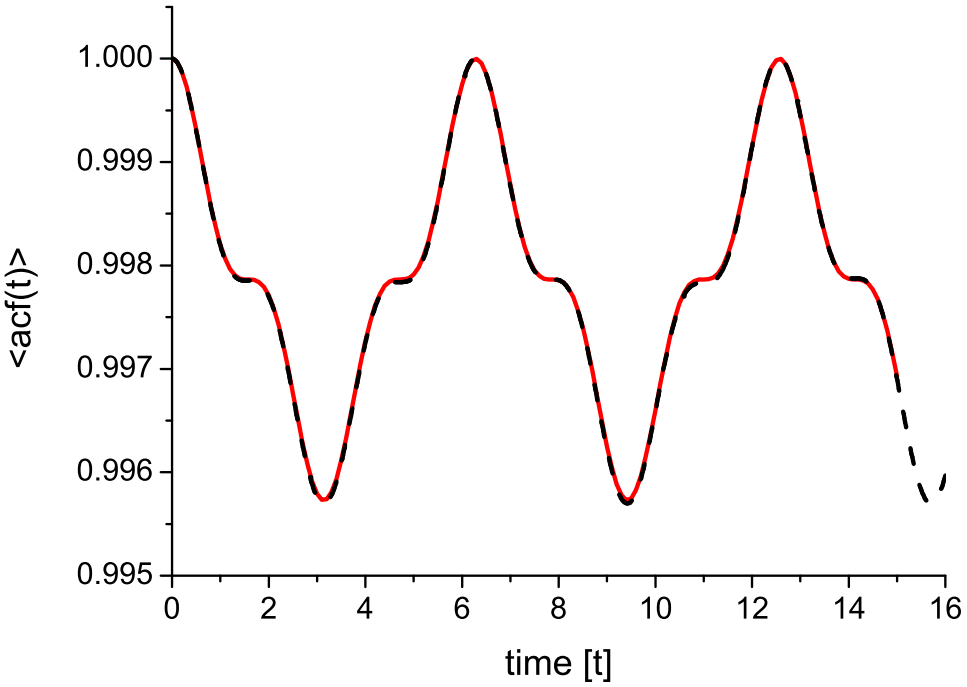

Figure 10. Plot of the autocorrelation function $\langle \mathrm{acf}(t) \rangle$ vs. t for a dimensionless temperature of $T = 0.00160156$. The red curve shows the analytical results; the black curve shows the numerical results.

$\langle \sqrt{(1-z_1(0)^2)(1-z_1(t)^2)}\cos(\phi_1(0)-\phi_1(t)) \rangle$ will probably not vanish since the phase shifts of the $x-y$-oscillations have been already canceled in the argument of the cos-function. This conjecture has to be confirmed by the detailed calculations.

These calculations can be simplified by the following consideration. The transformation $\boldsymbol{s}_i \mapsto -\boldsymbol{s}_i$, $i = 1, 2$, introduces a minus sign in the eom (8) and hence can be considered as a kind of "time reversal". However, it leaves the acf invariant and hence $\langle \mathrm{acf} \rangle$ will be also invariant under time reversal. Consequently, the terms of acf proportional to $\sin(t), \sin(2t)$ and $\sin(3t)$ will vanish in the thermal average and need not be calculated.

The calculation of $\langle \mathrm{acf}(t) \rangle$ is based on the approximation of the Hamiltonian H to terms at most quadratic in the deviations from a ground state. We do not give the details but the main steps are sketched in Appendix D. The final result reads:

$$\langle \mathrm{acf} \rangle = 1 - \frac{4}{3\beta} + \frac{3\cos(t) + \cos(3t)}{3\beta} + \mathcal{O}(\beta^{-2}) \,. \tag{82}$$

This shows that indeed the frequency $\omega = 2$ of the z_1-oscillation is suppressed by thermal averaging and can at most occur as contributions of order $\mathcal{O}(\beta^{-2})$.

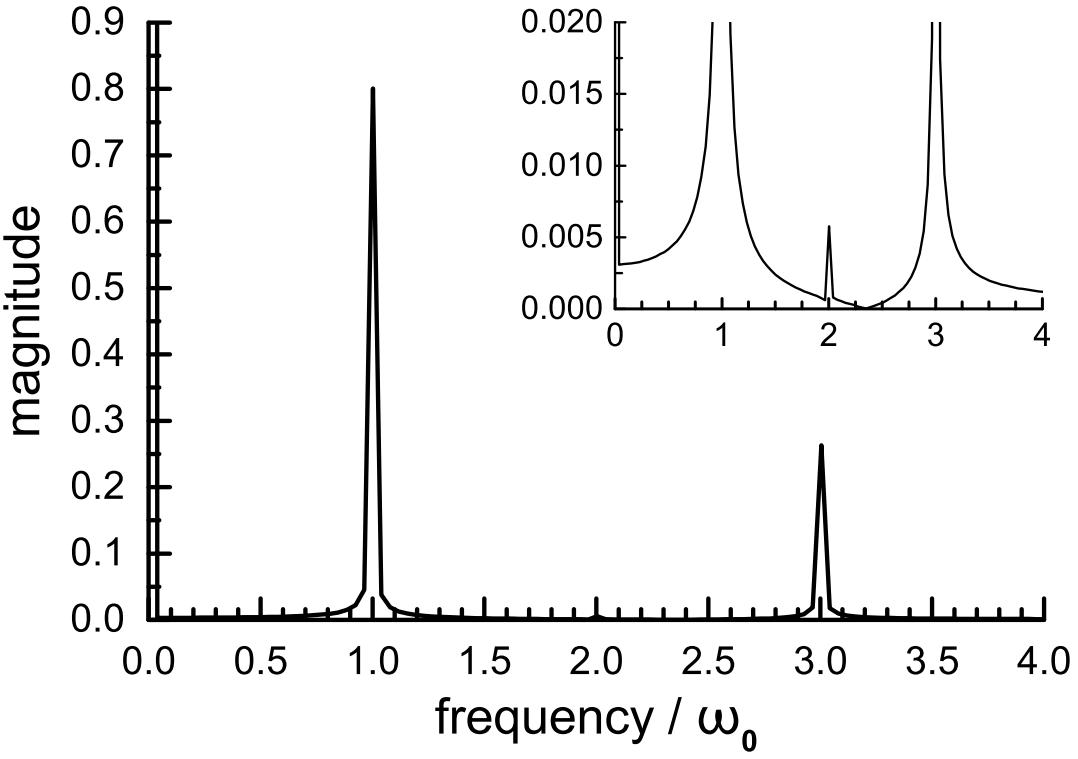

Figure 11. Plot of the Fourier transform of the autocorrelation function $\langle \mathrm{acf}(t) \rangle$ vs. ω for a dimensionless temperature of $T = 0.00160156$. The inset shows the peak at $\omega = 2$ which is almost suppressed by thermal averaging. The amplitudes of the two large peaks are in the ratio of $2.95 : 1$ in accordance with (82).

We compared these results with numerical simulations. In order to calculate the canonical ensemble average numerically we used the so-called "Gibbs approach" [29], where the trajectories $\boldsymbol{s}_1(t)$ for the dipoles are calculated for the *isolated* system by solving the equations of motion (8) and (9) over a certain number of time steps numerically. The initial conditions for each trajectory are generated by a standard Monte Carlo simulation for a temperature T. By averaging all generated trajectories at each time step one obtains the canonical ensemble average. In figure 10 we show a comparison of our analytical and simulation results in the time domain. The Fourier transform of the simulation data (see figure 11) yields the expected spectrum showing three distinct peaks, where the peak at the frequency $\omega = 2$ is almost suppressed compared to the other peaks.

3.6.2. Long time behavior It is known [29] that even for integrable systems such as the classical Heisenberg dimer the long time behavior of $\langle \mathrm{acf} \rangle$ is different from that for short times: The amplitude of the oscillation decays and for $t \to \infty$ the function $\langle \mathrm{acf} \rangle$ approaches a positive value depending on the temperature. The corresponding

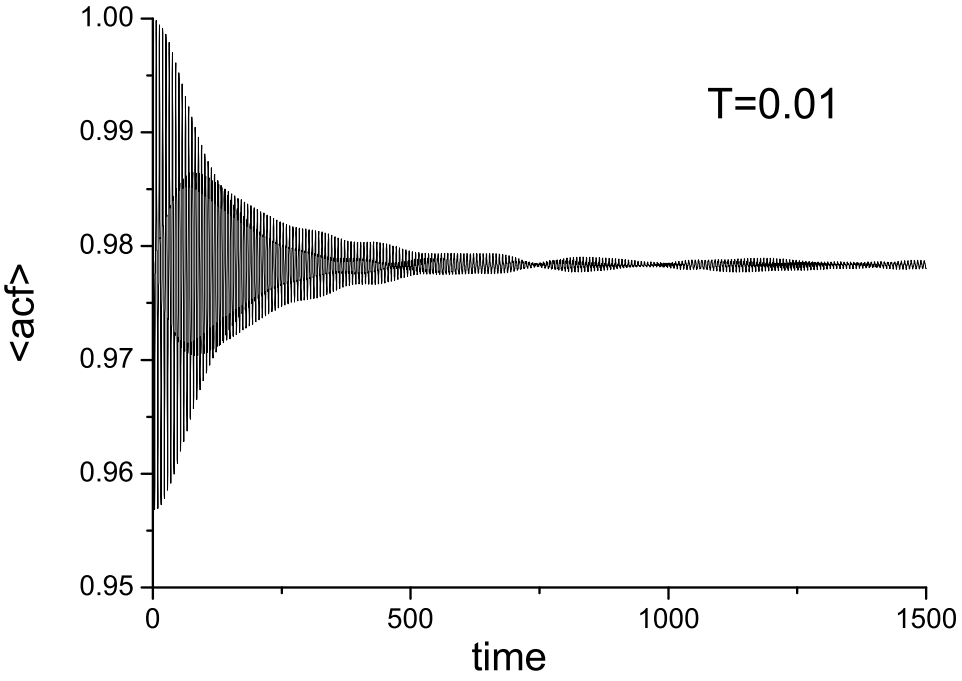

Figure 12. Plot of the long time behavior of $\langle \mathrm{acf} \rangle$ for a dimensionless temperature of $T = 0.01$. One observes a relaxation of $\langle \mathrm{acf} \rangle$ to the mean value of the initial oscillation.

relaxation time decreases with increasing temperature but has always a finite value. In our case the same effect occurs, see figure 12.

Our method to describe the short time behavior of $\langle \mathrm{acf} \rangle$, namely the harmonic oscillator approximation, is not suited to describe its relaxation occurring for times $t \gg P$, where P is the period of the oscillation of $z_i(t),\ i = 1, 2$. However, we can give a semi-quantitative explanation of the relaxation effect. Contrary to the harmonic oscillator approximation the two frequencies of the oscillation of $x_i(t)$ and $y_i(t),\ i = 1, 2$, will not be constant but vary with the values of the conserved quantities σ and ε, even for solutions close to the ground state(s). Let us consider the dominant part $\cos\left(a_0 + \frac{\delta}{P}\, t\right)$ of the oscillation of $x(t)$ with $\omega = \frac{\delta}{P} \approx -1$ and focus on the energy-dependence of ω. Using (C.14) and (31) and taking the limit $\sigma \to -2$ we obtain

$$\omega = \frac{\delta}{P} = -1 + \frac{5}{4}(\varepsilon - \varepsilon_0) + \mathcal{O}(\varepsilon - \varepsilon_0)^2 \,. \tag{83}$$

Moreover, we adopt the low energy asymptotic of the density of states

$$\rho(\varepsilon) = \frac{1}{6}(\varepsilon - \varepsilon_0) + \mathcal{O}(\varepsilon - \varepsilon_0)^2 \,, \tag{84}$$

that an be obtained from (50). Then, ignoring the phase shift a_0, we would expect the

low temperature thermal average of the oscillation $x(t) = \cos\left(\frac{\delta}{P}\,t\right)$ to be given by

$$\begin{aligned}\langle x(t)\rangle &= \left(\int_0^\infty \frac{\xi}{6}\exp(-\beta\xi)d\xi\right)^{-1}\int_0^\infty \frac{\xi}{6}\cos\left(\left(-1+\frac{5}{4}\xi\right)t\right)\exp(-\beta\xi)d\xi \\ &= \frac{16\beta^2\left(\left(16\beta^2-25t^2\right)\cos(t)+40t\beta\sin(t)\right)}{\left(25t^2+16\beta^2\right)^2} \qquad (85)\\ &= -\frac{16}{25}\left(\frac{\beta}{t}\right)^2\sin t+\frac{128}{125}\left(\frac{\beta}{t}\right)^3\cos t+\mathcal{O}(t^{-4})\,, \qquad (86)\end{aligned}$$

where we have substituted ξ for the variable $\varepsilon-\varepsilon_0$ and extended the integration to the whole positive domain $0\le\xi<\infty$. If the oscillating parts of $\langle\text{acf}\rangle$ decay for $t\to\infty$ only the constant part will survive. For low temperatures of, say, $T<0.001$ the limit of $\langle\text{acf}\rangle$ will hence be given by $1-4T/3$ according to (82) which is confirmed by numerical calculations. For larger T the limit of $\langle\text{acf}\rangle$ cannot longer be calculated by the harmonic oscillator approximation and will be lower than $1-4T/3$.

We stress that this is only a crude model for the relaxation of $\langle\text{acf}\rangle$, but we expect that the general result would be similar in two respects: namely (1) that the relaxation is of polynomial rather than exponential character and (2) that the leading amplitude terms would only depend on the ratio $\frac{\beta}{t}$. The latter explains the plausible result that the relaxation time increases with decreasing temperature. The long time simulations of $\langle\text{acf}\rangle$ that we have performed seem to confirm these conjectures.

4. Summary and Outlook

In this paper we have investigated the system consisting of two magnetic dipoles, fixed in space and interacting via its magnetic fields. The dynamics of this system has been completely resolved and the general solution of the equations of motion has been given in terms of elliptic integrals and Weierstrass elliptic functions. The thermodynamics of the two dipole system based on the canonical ensemble has also been determined by means of series expansions, including the low temperature limit of the autocorrelation function. The analytical results have been confirmed by numerical Monte Carlo simulations.

Hence we have found a simple but non-trivial example for a solvable system in the sense of classical mechanics and of classical thermodynamics based on the canonical ensemble for systems with small particle numbers. The other motif of our studies was to prepare the investigation of larger systems of interacting dipoles that have been recently realized by experimentalists. Therefore it is in order to reflect about possible generalizations of our methods to larger systems. First, it is clear that the Hamiltonian (21) can be directly generalized to systems of N dipoles and yields the corresponding Hamiltonian eom for the canonical coordinates $(p_i,\,q_i)=(\phi_i,\,z_i)$, $i=1,\ldots,N$. However, we do not expect that these eom are completely integrable for $N>2$ due to the lack of a sufficient number of integration constants. It is a typical situation in classical mechanics that the property of being completely integrable is satisfied for a

two-body-problem but gets lost for three or more particles. Nevertheless, it might be possible to find *some* exact solutions for larger systems of dipoles and to identify its ground states. In general, it will be difficult to find all ground states due to geometric frustration. However, for the special case of N dipoles sitting at the vertices of a regular polygon the two ground states can be shown to consist of magnetic moment vectors pointing in tangent direction relative to the circle circumscribed around the polygon. In those cases where the ground state(s) can be found, the linearization of the eom close to these should be possible and would only be practically limited by the size of N. Concerning thermodynamics, we are pessimistic about the possibility to generalize our series expansions to larger systems due to the complexity of the calculations. However, the "linear oscillator approximation" would still be possible and would yield low temperature limits of, e. g. , the autocorrelation function. Similar as for the dipole pair systems of larger dipole systems would show oscillatory behavior of the autocorrelation function $\langle \mathrm{acf}(t) \rangle$ at low temperatures and short times, and relaxation to finite values at long times. Moreover, the long–range of the dipolar interaction might induce specific behaviors, like trapping in quasi-stationary states. In view of the mentioned difficulties the role of numerical simulations would become more important for larger systems of magnetic dipoles.

Acknowledgment

E. H. and C. S. acknowledge financial support from the equal opportunity commissioner of the Bielefeld University of Applied Sciences. H.-J. S. is indebted to Hans-Werner Schürmann for discussions about Weierstrass elliptic functions.

Appendix A. Elliptic integrals and Weierstrass elliptic functions

There are many problems in theoretical physics that lead to elliptic integrals (EI) or their inverses, elliptic functions (EF). We only mention a few:

- Various problems of classical mechanics [30] including one-dimensional motion of a particle in a cubic or quartic potential, the spherical pendulum or the spinning top,
- the magnetic field of a circular current loop [31], Ch. 5,
- the TE field in a slab filled with a Kerr non-linear medium [32],
- certain solutions of the Korteweg-de-Vries equation [30], and
- a correspondence between Bose-Einstein condensates and problems from cosmology [33].

Nevertheless, most authors of physics textbooks seem to refrain from the use of these special functions, one exception being the above-cited [31]. This is the more regrettable since by utilizing computer algebra software both EI and EF can be evaluated with the same ease as, say, the sin and arcsin functions.

Here we cannot give an extended introduction into the field but will rather sketch the fundamental ideas. One can understand the EI and EF as generalizations of the well-known "circular case", where one encounters the elementary integral

$$t = \int \frac{dx}{\sqrt{1-x^2}} = \arcsin x \ + \ t_0 \ , \tag{A.1}$$

defined for $-1 \leq x \leq 1$ and its inverse function

$$x(t) = \sin(t - t_0) \ , \tag{A.2}$$

that can be extended to a periodic function defined for all $-\infty < t < \infty$. The following generalization of (A.1) is the *incomplete EI of the first kind*:

$$t = \int_0^x \frac{dx}{\sqrt{(1-x^2)(1-mx^2)}} \equiv F(\arcsin x, m) \ . \tag{A.3}$$

By the *complete EI of the first kind* one denotes the special case of the integral

$$\int_0^1 \frac{dx}{\sqrt{(1-x^2)(1-mx^2)}} \equiv K(m) \ , \tag{A.4}$$

that can be used, e. g. , for calculating the period of oscillation of a pendulum.

More generally, it can be shown [28], Ch. 17, that any integral of a rational function of x and $\sqrt{P(x)}$, where $P(x)$ is a polynomial of at most 4th degree, can be expressed in terms of elementary functions and the so-called EI of first, second or third kind.

Similarly as in the circular case, one is often interested in the function $x(t)$ rather than $t(x)$, that is, for the periodic extension of the inverse function of the EI, the EF. There exist different versions of the EF; in this paper we will use the Weierstrass EF, $u = \mathcal{P}(z; g_2, g_3)$. It is first defined by inverting

$$z = \int_\infty^u \frac{dv}{\sqrt{P(v)}} \ , \tag{A.5}$$

where $P(v) = 4v^3 - g_2 v - g_3$. Then $\mathcal{P}$ is extended to a doubly periodic complex function, analytic in the whole complex plane except for the pole at $z = 0$ and its translates. For more details, see Chapter 18 of [28] and an introduction to the theory as it is given, e. g. , in [30] or [34].

Appendix B. Exact solution for $z_1(t)$

The first step is to eliminate z_2 and $\phi_1 - \phi_2$ from (19) by using the constants $\boldsymbol{S} \cdot \boldsymbol{e} = \sigma$ and $H = \varepsilon$. We write $z_1 = z$. The result is

$$\dot{z} \quad = \sqrt{-3Q_+Q_-} \ , \tag{B.1}$$

where

$$Q_\pm \quad \equiv \frac{1}{3}\left(1 - 2\varepsilon - 3\sigma z + 3z^2 \pm \sqrt{\varepsilon^2 - 4\varepsilon - 3\sigma^2 + 4}\right) . \tag{B.2}$$

Upon substituting

$$v = (2z-\sigma)^2 - v_0 \,, \tag{B.3}$$

$$v_0 \equiv \frac{2}{9}\left(8\varepsilon + 3\sigma^2 - 4\right) \tag{B.4}$$

we obtain

$$t = \int \frac{dz}{\sqrt{-3Q_+Q_-}} = \frac{2}{\sqrt{-3}} \int \frac{dv}{\sqrt{4v^3 - g_2 v - g_3}} \,, \tag{B.5}$$

with g_2 and g_3 according to (25) and (26). Inserting appropriate boundaries and writing $4v^3 - g_2 v - g_3 = P(v)$ we have

$$\frac{i\sqrt{3}}{2}t = \int_{-v_0}^{(2z-\sigma)^2-v_0} \frac{dv}{\sqrt{P(v)}} \tag{B.6}$$

$$= \int_{\infty}^{(2z-\sigma)^2-v_0} \frac{dv}{\sqrt{P(v)}} - \int_{\infty}^{-v_0} \frac{dv}{\sqrt{P(v)}} \tag{B.7}$$

$$\equiv u_1 - u_2 \,. \tag{B.8}$$

According to the definition of the Weierstrass $\mathcal{P}$-function, this is equivalent to

$$\mathcal{P}(u_1) = (2z-\sigma)^2 - v_0 = (2z-\sigma)^2 + \mathcal{P}(u_2) \,, \tag{B.9}$$

or, solving for z,

$$z(t) = \frac{1}{2}\left(\sigma \pm \sqrt{\mathcal{P}(u_1) - \mathcal{P}(u_2)}\right) \tag{B.10}$$

$$= \frac{1}{2}\left(\sigma \pm \sqrt{\mathcal{P}\left(\frac{i\sqrt{3}}{2}t + u_2\right) - \mathcal{P}(u_2)}\right) \,. \tag{B.11}$$

This confirms (31). As a consequence of choosing the lower boundary of the integral (B.6) to be $-v_0$ we have $z(0) = \sigma/2$. For a more general solution one can simply replace t in the r. h. s. of (B.11) by $t - t_0$.

Appendix C. Exact solution for $\phi_{1,2}(t)$

We write $z = z_{1,2},\ \phi = \phi_{1,2}$ and have to solve the integral

$$\int d\phi = \int \frac{\dot{\phi}}{\dot{z}} dz \,, \tag{C.1}$$

where $\dot{\phi}$ and $\dot{z}$ have to be inserted from (32) and (B.1).
Defining

$$a_0 = -\sigma\sqrt{-3v_-} \,, \tag{C.2}$$

$$a_1 = 2\sqrt{-3v_-} \,, \tag{C.3}$$

$$\mu = -\frac{1}{16}\left(4\varepsilon + \sigma^2 + 4\right)\left(4\varepsilon + 3\sigma^2 - 4\right) \,, \tag{C.4}$$

$$m = \frac{v_+}{v_-} \,, \tag{C.5}$$

the substitution $x = a_1\, z + a_0$ yields

$$\frac{dz}{\dot{z}} = \frac{dz}{\sqrt{-3Q_+Q_-}} = \frac{dx}{a_1\sqrt{\mu}\sqrt{(1-x^2)\,(1-mx^2)}}\,. \tag{C.6}$$

Upon this substitution (32) can be written as

$$\dot{\phi} = \frac{(\varepsilon-2)z + 2\sigma}{z^2-1} = \frac{A_+}{1-n_+x} + \frac{A_-}{1-n_-x}\,, \tag{C.7}$$

where

$$A_\pm = \frac{-2+\varepsilon \mp 2\sigma}{\pm 2+\sigma}\,, \tag{C.8}$$

$$n_\pm \;=\; \mp\,\frac{1}{\sqrt{-3v_-}(2\pm\sigma)}\,. \tag{C.9}$$

These transformations lead to writing (C.1) as a sum of two integrals of the form

$$W\,(n;\,x|\,m) \equiv \int \frac{dx}{(1-nx)\sqrt{(1-x^2)\,(1-mx^2)}}\,. \tag{C.10}$$

Writing

$$\frac{1}{(1-nx)} = \frac{1}{1-n^2x^2} + \frac{n\,x}{1-n^2x^2}\,, \tag{C.11}$$

we obtain

$$\begin{aligned} &W\,(n;\,x|\,m) = \\ &\Pi\left(n^2;\,\sin^{-1}(x)\Big|\,m\right) - \frac{n}{\sqrt{1-n^2}\sqrt{n^2-m}}\tan^{-1}\left(\frac{\sqrt{1-x^2}\sqrt{n^2-m}}{\sqrt{1-mx^2}\sqrt{1-n^2}}\right)\,, \end{aligned} \tag{C.12}$$

where Π is the incomplete elliptic integral of third kind, see [28] Ch. 17. The final result reads

$$\phi(t) = \phi_0 \pm \frac{1}{a_1\sqrt{\mu}}\;\left(A_+W\,(n_+;\,a_1z(t)+a_0|\,m) + A_-W\,(n_-;\,a_1z(t)+a_0|\,m)\right), \tag{C.13}$$

where the constant ϕ_0 and the sign $\pm$ have to be chosen in such a way that (C.13) piecewise coincides with the correct solution $\phi(t)$, see figure 2. As a rule, ϕ_0 and the sign $\pm$ have to be changed if the argument x in $W\,(n;\,x|\,m)$ touches the extremal values ± 1. It is then a straight-forward task to calculate the drift δ of the azimuthal angle ϕ during one period P, see figure 2 and the corresponding remarks in subsection 2.2. The result is

$$\delta \;=\; \frac{-4}{a_1\sqrt{\mu}}\left(A_+\Pi(n_+^2\Big|\,m) + A_-\Pi(n_-^2\Big|\,m)\right), \tag{C.14}$$

where $\Pi(n^2|\,m)$ denotes the complete elliptic integral of third kind, see [28], Ch. 17.

Appendix D. Low temperature limit of $\langle \mathrm{acf}(t)\rangle$ for short times

For the calculation of the low temperature limit of $\langle \mathrm{acf}(t)\rangle$ we write for the magnetic moments close to one of the ground states, analogously to (39),

$$\boldsymbol{s}_1 = \begin{pmatrix} X_1 \\ X_2 \\ -1+\frac{1}{2}(X_1^2+X_2^2) \end{pmatrix}, \quad \boldsymbol{s}_2 = \begin{pmatrix} X_3 \\ X_4 \\ -1+\frac{1}{2}(X_3^2+X_4^2) \end{pmatrix}, \tag{D.1}$$

and evaluate H up to second order in $|\boldsymbol{X}|$. The result can be written as

$$H_2 \equiv -2 + \boldsymbol{X}\cdot\boldsymbol{M}\cdot\boldsymbol{X}\ , \tag{D.2}$$

where

$$\boldsymbol{M} = \begin{pmatrix} 1 & 0 & \frac{1}{2} & 0 \\ 0 & 1 & 0 & \frac{1}{2} \\ \frac{1}{2} & 0 & 1 & 0 \\ 0 & \frac{1}{2} & 0 & 1 \end{pmatrix}\ . \tag{D.3}$$

The eigenvalues of the symmetric matrix $\boldsymbol{M}$ are $M_{1,2}=\frac{3}{2},\ M_{3,4}=\frac{1}{2}$. They are positive in accordance with the fact that the considered ground state realizes the energy minimum $\varepsilon_0=-2$. Their values are exactly 1/2 of the two basic frequencies $\omega_1=1,\ \omega_2=3$, i. e. , of the absolute values of the eigenvalues of $\boldsymbol{A}$, see (41). We perform a rotation into the eigenbasis of $\boldsymbol{M}$ and call the new coordinates Y_i, $i=1,\ldots,4$. In the second order approximation w. r. t. $|\boldsymbol{X}|$ we then obtain the partition function

$$\frac{1}{2}Z(\beta) \sim e^{2\beta}\frac{1}{(4\pi)^2}\prod_{i=1}^{4}\int_{-\infty}^{\infty}\exp\left(-\beta M_i Y_i^2\right)\,dY_i = \frac{e^{2\beta}}{12\beta^2}\ , \tag{D.4}$$

which confirms the result (64) obtained by a different method. Recall that the factor $\frac{1}{2}$ is introduced since the second ground state gives the same contribution to $Z(\beta)$.

The present method is also suited to calculate the low temperature limit of $\langle \mathrm{acf}(t)\rangle$ for short times, i. e. , for times t comparable with the period P of oscillations (31). Consider first

$$\mathrm{acf}_1(t) \equiv X_1(0)\,X_1(t) \tag{D.5}$$

$$= \frac{1}{2}(Y_2-Y_4)\times(-Y_1\sin 3t + Y_3\sin t + Y_2\cos 3t - Y_4\cos t). \tag{D.6}$$

If this expression is inserted into the integrals (D.4) only those terms survive that are quadratic in the Y_i, namely $\frac{1}{2}\,(Y_2^2\cos 3t + Y_4^2\cos t)$. Upon division by $\frac{1}{2}Z(\beta)$ we obtain

$$\langle \mathrm{acf}_1(t)\rangle = \frac{2}{3\beta}\cos^3 t + \mathcal{O}(\beta^{-2})\ . \tag{D.7}$$

By azimuthal symmetry $\langle \mathrm{acf}_2(t)\rangle \equiv \langle X_2(0)\,X_2(t)\rangle = \langle \mathrm{acf}_1(t)\rangle$. For $\langle \mathrm{acf}_3(t)\rangle$ we have

$$\langle \mathrm{acf}_3(t)\rangle \equiv \langle\ (-1+\frac{1}{2}(X_1(0)^2+X_2(0)^2))(-1+\frac{1}{2}(X_1(t)^2+X_2(t)^2))\ \rangle \tag{D.8}$$

$$= 1 - \frac{1}{2}\langle(X_1(0)^2+X_2(0)^2)\rangle - \frac{1}{2}\langle(X_1(t)^2+X_2(t)^2)\rangle + \mathcal{O}(\beta^{-2}). \tag{D.9}$$

and by the same method as above it follows that the thermal average of the time-dependent terms vanishes such that

$$\langle \mathrm{acf}_3(t) \rangle = 1 - \frac{4}{3\beta} + \mathcal{O}(\beta^{-2}) \; . \tag{D.10}$$

Adding all contributions to $\langle \mathrm{acf}(t) \rangle$ we obtain the following expression which proves (82):

$$\langle \mathrm{acf}(t) \rangle = 1 - \frac{4}{3\beta} + \frac{4}{3\beta} \cos^3 t + \mathcal{O}(\beta^{-2}) \tag{D.11}$$

$$= 1 - \frac{4}{3\beta} + \frac{3\cos(t) + \cos(3t)}{3\beta} + \mathcal{O}(\beta^{-2}) \; . \tag{D.12}$$

References

[1] Franco A F, Déjardin J L and Kachkachi H 2014 *J. Appl. Phys.* **116** 243905

[2] Ewerlin M, Demirbas D, Brüssing F, Petracic O, Ünal A A, Valencia S, Kronast F and Zabel H 2013 *Phys. Rev. Lett.* **110** 177209

[3] Miloshevich G, Dauxois T, Khomeriki R and Ruffo S 2013 *Eur. Phys. Lett.* **104** 17011

[4] Varon M, Beleggia M, Kasama T, Harrison R J, Dunin-Borkowski R E, Puntes V F and Frandsen C 2013 *Sci. Rep.* **3** 1234

[5] Dzyan S A and Ivanov B A 2013 *Low Temp. Phys.* **39** 525–529

[6] Dzyan S A and Ivanov B A 2013 *JETP* **116** 975–979

[7] Wunsch B, Zinner N T, Mekhov I B, Huang S–J, Wang D–J and Demler E 2011 *Phys. Rev. Lett.* **107** 073201

[8] Stuhler J, Griesmaier A, Koch T, Fattori M, Pfau T, Giovanazzi S, Pedri P and Santos L 2005 *Phys. Rev. Lett.* **95** 150406

[9] Unold T, Mueller K, Lienau Ch, Elsaesser T and Wieck A D 2005 *Phys. Rev. Lett.* **94** 137404

[10] Jonsson T, Nordblad P and Svedlindh P 1998 *Phys. Rev. B* **57** 497–594

[11] Wang R F, Nisoli C, Freitas R S, Li J, McConville W, Cooley B J, Lund M S, Samarth N, Leighton C, Crespi V H and P. Schiffer P 2006 *Nature* **439** 303-306

[12] Castelnovo C, Moessner R and Sondhi S L 2008 *Nature* **451** 06433

[13] Hiroi K, Komatsu K and Sato T 2011 *Phys. Rev. B* **83** 224423

[14] Imre A, Csaba G, Ji L, Orlov A, Bernstein G H and Porod W 2006 *Science* **311** 205-208

[15] Eichwald I, Breitkreutz S, Ziemys G, Csaba G, Porod W and Becherer M 2014 *Nanotechnology* **25** 335202

[16] Campa A, Dauxois T, and Ruffo S 2009 *Phys. Rep.* **480** 57–159

[17] Hukushima K and Nemoto K 1996 *J. Phys. Soc. Jpn.* **65** 1604–1608

[18] Spaldin N A 2010 *Magnetic Materials: Fundamentals and Applications* (Cambridge: Cambridge University Press)

[19] It is shown in [20], Problems 5.11 and 5.36, that the magnetic field outside a spinning shell is a perfect dipole field. On the other hand, we could not find any reference to the exact validity of (3) for this system and hence will give the proof in a forthcoming publication.

[20] Griffith D J 1999 *Introduction to Electrodynamics* 3rd ed (Upper Saddle River: Prentice Hall)

[21] Arnol'd V I 1978 *Mathematical Methods of Classical Mechanics* (Berlin: Springer)

[22] Miloshevich G, Dauxois T, Khomeriki R and Ruffo S 2013 *Eur. Phys. Lett.* **106** 140405

[23] Cassidy A C, Clark C W and Rigol M 2011 *Phys. Rev. Lett.* **104** 17011

[24] Wang F and Landau D P 2001 *Phys. Rev. Lett.* **86** 2050

[25] Jones D S 2007 *Proc. Edinburgh Math. Soc.* **50** 173

[26] As the notation "Tr" indicates, it can be shown [27] that the normalized volume integral of f over phase space equals the classical limit of the corresponding normalized trace $\mathrm{tr}(F)/\mathrm{tr}(\mathbb{1})$.

[27] Lieb E H 1973 *Commun. Math. Phys.* **31** 327
[28] Abramowitz M and Stegun I A 1972 (eds) *Handbook of Mathematical Functions* (New York: Dover)
[29] Luban M and Luscombe J H 1999 *Am. J. Phys.* **67** 1161–1169
[30] Brizard A J 2009 *Eur. J. Phys.* **30** 729-750
[31] Jackson J D 1999 *Classical Electrodynamics* 3rd ed (Hoboken: Wiley)
[32] Schürmann H–W 1995 *Z. Phys.* B **97** 515–522
[33] D´Ambroise J and Williams F L 2010 *J. Math. Phys.* **51** 062501
[34] Bowman F 1961 *Introduction to elliptic functions* (New York: Dover)